2. The histopathological changes in the trabecular outflow pathway and their possible effects on aqueous outflow in eyes with primary open-angle glaucoma

Haiyan Gong, David L. Swain

Boston University School of Medicine, Boston, MA, USA

1. Introduction

Primary open-angle glaucoma (POAG) is an age-related disease and a multifaceted optic neuropathy characterized by the loss of optic nerve axons and retinal ganglion cells. A primary risk factor for the development and progression of this disease is elevation of the intraocular pressure (IOP),[1] resulting from increased resistance to aqueous humor outflow in the aqueous outflow pathway.[2] Normal IOP is maintained through a dynamic balance between aqueous production and drainage. The trabecular or conventional outflow pathway is the major drainage pathway of aqueous humor[3-5] and is comprised of the trabecular meshwork (TM), which includes the uveal meshwork, corneoscleral meshwork, and connective tissue, Schlemm's canal (SC), collector channels, the intrascleral venous plexus, and episcleral veins (Fig. 1). The biological changes in the cells and the extracellular matrix (ECM) that compromise this pathway advance with age and in POAG. These changes play a role in the pathogenesis of POAG and may contribute to an increase in outflow resistance and IOP. This chapter will discuss six histopathological changes in the trabecular outflow pathway that are found associated with POAG and their relationship with reduced active flow area, as well as potential new therapeutic targets to lower IOP in POAG.

2. A decrease in TM cellularity

Trabecular beams, both uveal and corneoscleral, consist of a central connective tissue core that is enveloped in a continuous wrapping of thin endothelial cells and a subcellular basal lamina (Fig.2). The trabecular cells produce and degrade the ECM composed of the trabecular beams.[6-11] Trabecular cells are phagocytic[12] and capable of removing endogenous and exogenous[13,14] particles to keep the trabecular outflow channels free of potentially obstructive debris. A progressive age-related loss of the TM cells has been reported in healthy eyes, but cellular loss beyond that of normal aging has been found in the TM of eyes with POAG (Fig. 3).[13,15,16] Most of the cell loss occurs during the fetal and postnatal periods, leveling off to a linear decline that continues through adult life.[15,16] In one study, the cell count decreased from ages 20 to 80 from 763,000 to 403,000 cells at an average rate of 6,000 cells per year.[13] The rate of cell loss appears to be similar in normal and POAG eyes, shown by their parallel cellularity curves in Figure 3.[16] However, POAG eyes have been shown to have a higher prevalence of apoptotic cells in the TM.[17] This loss of cells is thought to lead to increased local stiffness of the TM,[18-20] and the observed fusion of trabecular beams in eyes with advanced POAG may result from adhesions between denuded portions of adjacent trabecular beams (Fig. 4).

Correspondence: Prof. Haiyan Gong, MD, PhD, Department of Ophthalmology, Anatomy and Neurobiology, Boston University School of Medicine, 72 East Concord Street, L-905, Boston, MA 02118, USA.
E-mail: hgong@bu.edu

Glaucoma Research and Clinical Advances: 2016 to 2018, pp. 17-40
Edited by P.A. Knepper and J.R. Samples

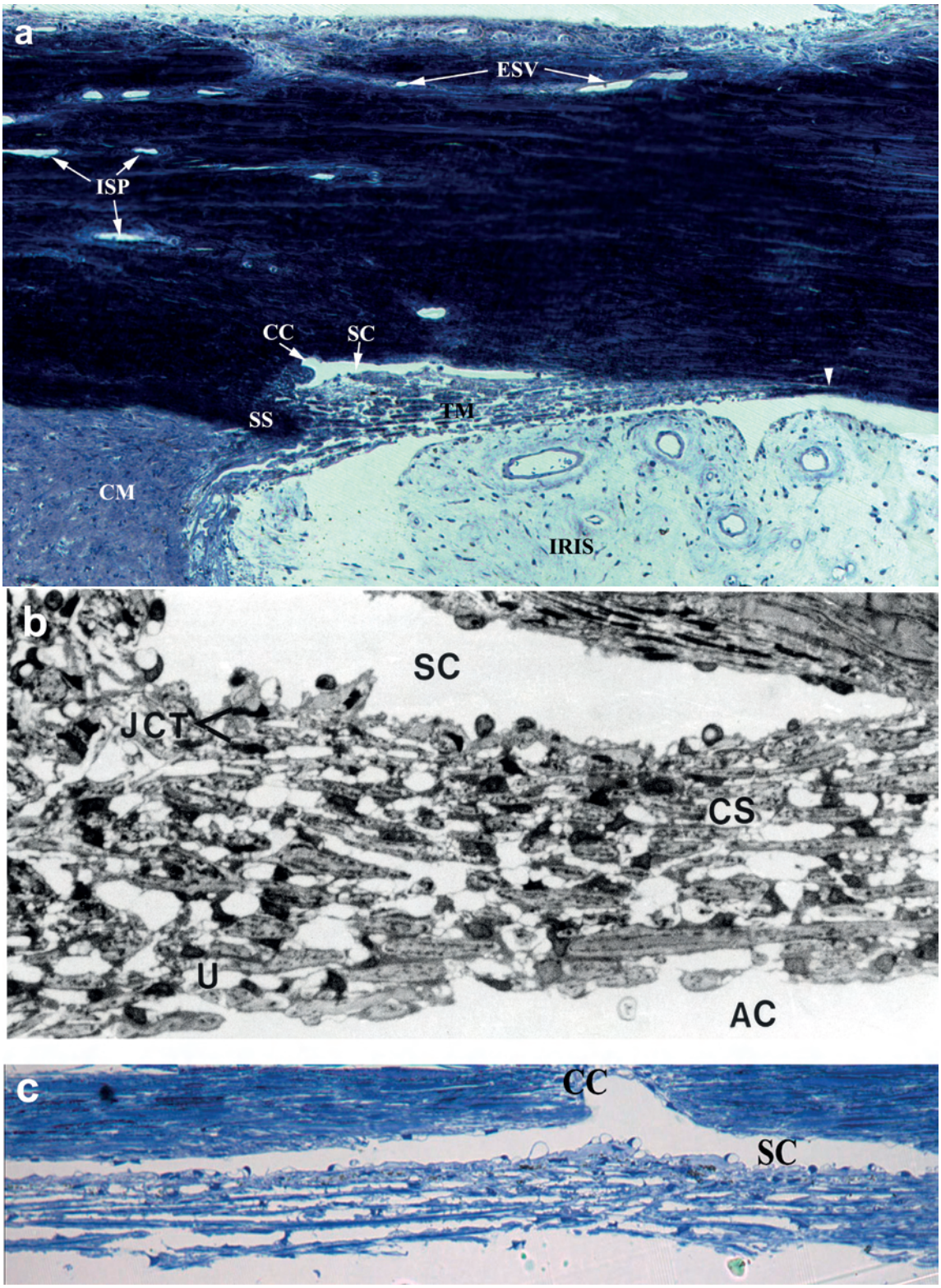

Fig. 1. Normal trabecular outflow pathway. **a.** A light micrograph of the anterior chamber angle is shown. Trabecular meshwork (TM), Schlemm's canal (SC), collector channel (CC), intrascleral plexus (ISP), episcleral vessels (ESV), scleral spur (SS), the ciliary muscle (CM), and iris are labeled. White arrowhead demarcates the terminus of Descemet's membrane, also known as Schwalbe's line. (Image provided by Haiyan Gong.) **b.** The trabecular meshwork is shown. From proximal to distal, the uveal trabecular meshwork (U), the corneoscleral trabecular meshwork (CS), and the juxtacanalicular tissue (JCT) are labeled. The anterior chamber (AC) and Schlemm's canal (SC) are also labeled. (Modified from Gong H, Freddo TF, Johnson M. Age-related changes of sulfated proteoglycans in the normal human trabecular meshwork. Exp Eye Res 1992;55,691-709.) **c.** A light micrograph of a coronal section of the trabecular meshwork is shown. Schlemm's canal (SC) and a collector channel (CC) are labeled. (Image provided by Haiyan Gong.)

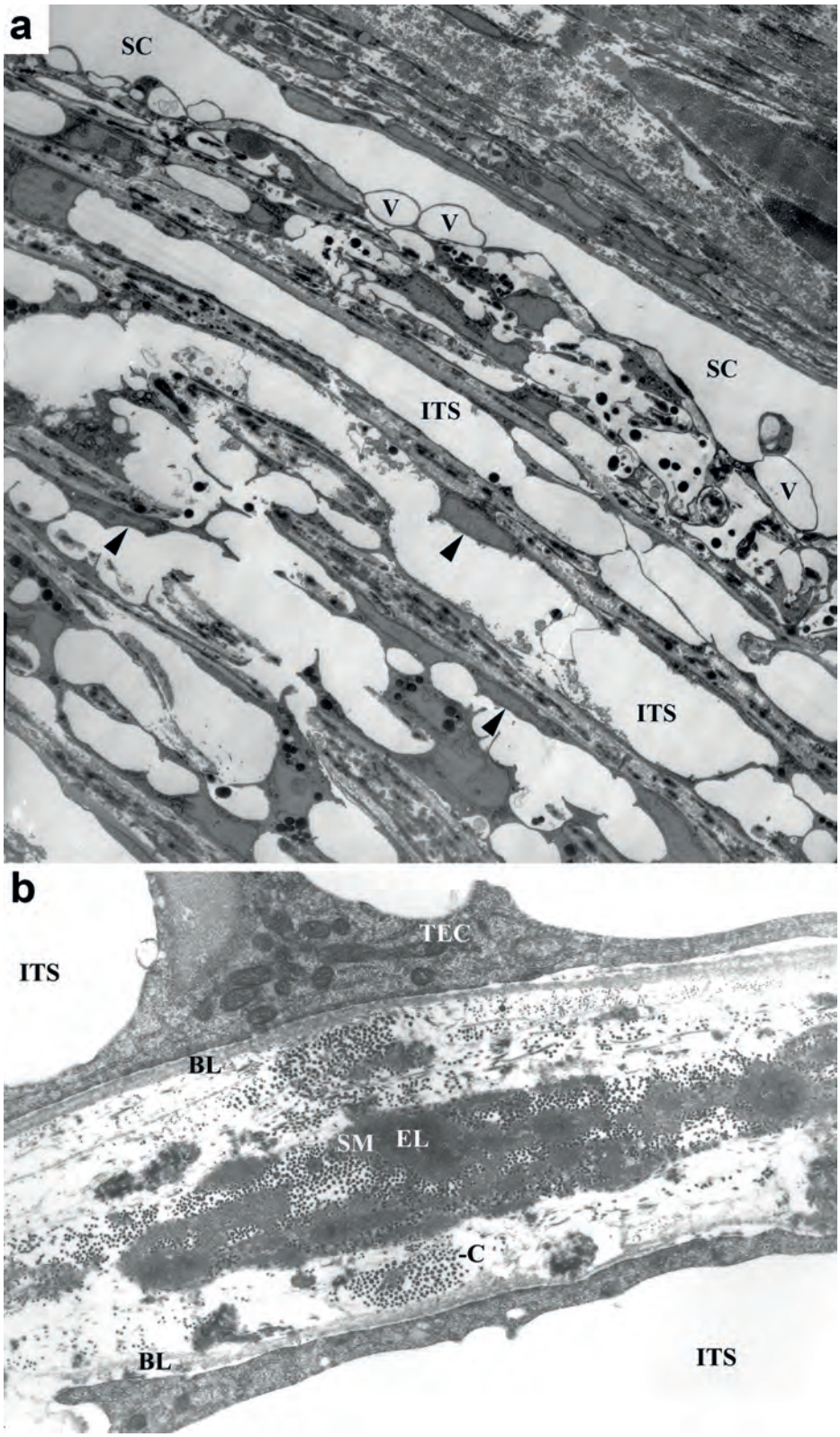

Fig. 2. Normal trabecular meshwork and trabecular beams. **a.** A transmission electron micrograph showing the trabecular meshwork from a 61-year-old donor eye, perfusion-fixed at 15 mmHg. Most beams are covered with endothelial cells (arrowheads). Giant vacuoles (V) are seen along the inner wall of SC. ITS = intertrabecular spaces. (Image provided by Haiyan Gong.) **b.** A transmission electron micrograph showing a cross-section of a normal trabecular beam. The trabecular beam is covered by a single layer of trabecular endothelial cells (TEC) that rest on the basal lamina (BL), which surrounds a central connective tissue core. C = collagen; EL = elastic fiber; SM = sheath material of elastic fiber; ITS = intertrabecular spaces. (From Gong *et al.* A new view of the human trabecular meshwork using quick-freeze, deep-etch electron microscopy. Exp Eye Res 2002; 75:347-358.)

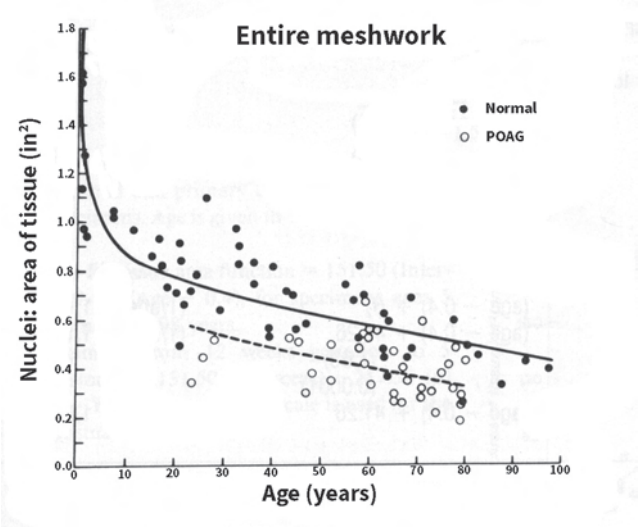

Fig.3. A linear decrease of TM cells was observed with age through adulthood. Normal (solid line) and POAG (broken line) show similar rates during adulthood, but there is greater TM cell loss in the eyes with POAG compared to normal aging. (From Alvarado *et al.* Trabecular meshwork cellularity in primary open-angle glaucoma and nonglaucomatous normals. Ophthalmology 1984; 91:564-579.)

Patients with severe loss of TM cells in advanced glaucoma may not respond well to the new glaucoma drugs that are currently under development and aim to target TM cells. Following laser trabeculoplasty, an increase in TM cell division has been reported in the anterior, non-filtration area of the TM, suggesting its regenerative capacity.[21] Currently, several studies are exploring the potential of a cell-based treatment to repopulate the TM with human TM stem cells and to restore its function. One study has shown functional phagocytic properties of TM cells after differentiation from TM stem cells.[22] Additionally, a TM cell loss model has been developed using perfusion with saponin detergents in a human anterior segment organ culture model to study the role of pluripotent stem cells in restoring the IOP homeostatic function of the TM.[23] Other studies have shown the efficacy of mouse models to study the function-restoring potential by TM stem cell replacement after laser injury[24] and that human TM

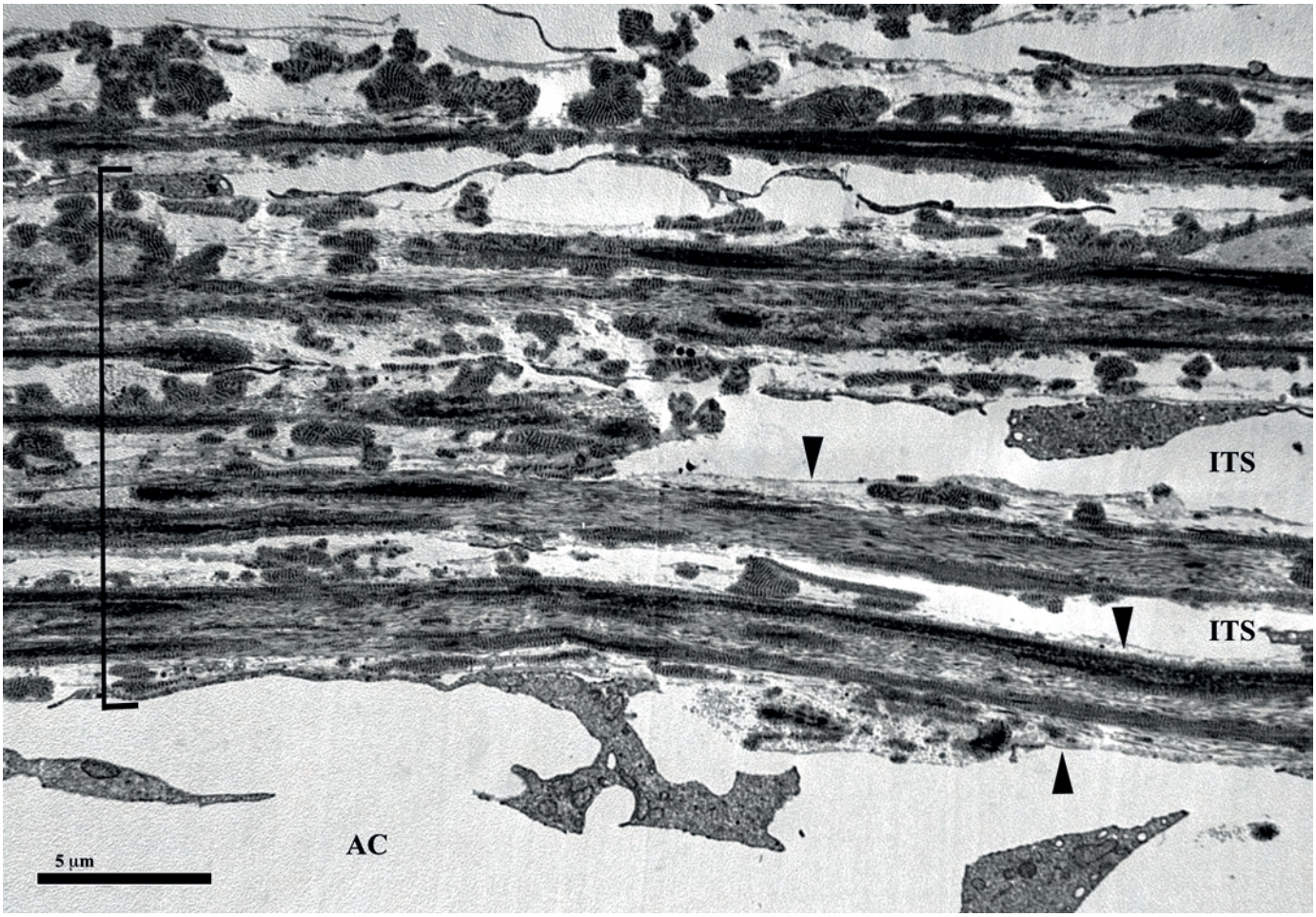

*Fig. 4. TM cell loss in POAG***.** A transmission electron micrograph from an eye with POAG showing a loss of cellularity and more 'naked' trabecular beams (arrowheads). Additionally, the decrease in cellularity causes the fusion of trabecular beams to one another (bracket). ITS = intertrabecular spaces; AC = anterior chamber. (Image provided by Haiyan Gong.)

stem cells are able to home to the TM in normal mice after injection into the anterior chamber.[25]

3. An abnormal accumulation of ECM

An increase in the amount of ECM including basement membrane and/or 'plaque material' in the juxtacanalicular connective tissue (JCT) has been reported in eyes with POAG (Fig. 5), whether or not they are receiving medical treatment.[26-28] This change is associated with increasing severity of optic nerve damage,[29] but morphometric studies of such specimens have been unable to account for the greater outflow resistance in POAG.[26] Numerous studies have demonstrated that transforming growth factor-β2 (TGF-β2) is elevated in the aqueous humor of patients with POAG.[30-34] High levels of TGF-β2 promote ECM formation and inhibit ECM degradation in the TM, both of which contribute to an increase in outflow resistance and IOP.[35-39] A significant accumulation of ECM molecules, including type VI collagen, fibronectin, and laminin, has been reported with age and in POAG, resulting in thickening of the trabecular beams;[6] increased type VI collagen, long-spacing collagen, has been observed in the subendothelial region of the trabecular beams with age and in POAG eyes[6] (Fig. 6). In those beams, the increased long-spacing collagen fibers are often associated with the TM cell loss; further studies will be needed to understand the relationship between the cell loss and the increase of type VI collagen.

4. A decrease in giant vacuoles and pores of the inner wall endothelial cells of Schlemm's canal

Aqueous humor must traverse the monolayer of continuous endothelial lining of Schlemm's canal (SC) from the JCT to enter the lumen. Exactly how aqueous humor traverses the endothelium of SC remains one of the enigmatic problems of ocular anatomy and physiology. A characteristic aspect of the inner wall endothelium of SC is the formation of giant vacuoles and pores. These vacuoles appear to be pressure-dependent and are not found unless the inner wall is fixed under conditions of active flow.[40] More giant vacuoles were observed near the collector channel ostia where preferential flow was reported.[41] Aqueous humor is believed to traverse the inner wall of SC though small openings or pores.[42] There are two types of pores, intracellular and paracellular pores (Fig. 7).[43] Intercellular pores (I pores) are often associated with giant vacuoles with a size between 0.1- 0.2 μm.[44] Paracellular pores (border pores or B pores) are located at the border between two adjacent endothelial cells of similar size. Pores are reported to be responsible for about 10% of the total outflow resistance in normal eyes.[44] One recent study identified that pores are not empty but filled with glycocalyx (Fig. 8).[45] A glycocalyx-filled pore has a far higher flow resistance than an empty pore, and therefore, the glycocalyx filling the pores could play a role in regulating aqueous outflow resistance.

Eyes with POAG exhibit fewer giant vacuoles[46] and pores[47,48] in the inner wall of SC than do healthy eyes (Fig. 9). This finding suggests that the endothelial cells lining SC lose their ability to passively permit aqueous humor to enter the lumen of the canal, possibly contributing to increased outflow resistance in eyes with POAG. Also, SC inner wall endothelial cell count decreases with increasing age at an average rate of 320 cells per year, which has been linked to a progressive reduction in vacuole count with age and a reduction in the size of SC.[49,50] Stiffness of the TM tissue in glaucomatous eyes was observed to be significantly higher than that in healthy eyes,[18-20] which may also partially account for the decreased ability of the inner wall endothelial cells to form giant vacuoles and pores. Recent cell culture studies have shown that SC endothelial cells from glaucomatous eyes have decreased pore-forming capability compared to those from healthy eyes, and this decreased pore-forming capability is correlated with increased cellular stiffness,[51] which may contribute to a decreased ability to modulate aqueous outflow and control IOP.[52] More interestingly, agents that increase (or decrease) stiffness of SC endothelial cells also increase (or decrease) outflow resistance.[53] These observations suggest the potential to develop a therapeutic approach to target SC endothelial cell stiffness to lower outflow resistance.

5. A shorter scleral spur

The scleral spur is a ridge-like projection of the sclera that provides an anchoring support for the ciliary muscle to act on and change the conformation of the TM, while also supporting and preventing collapse of SC.[54] To do this,

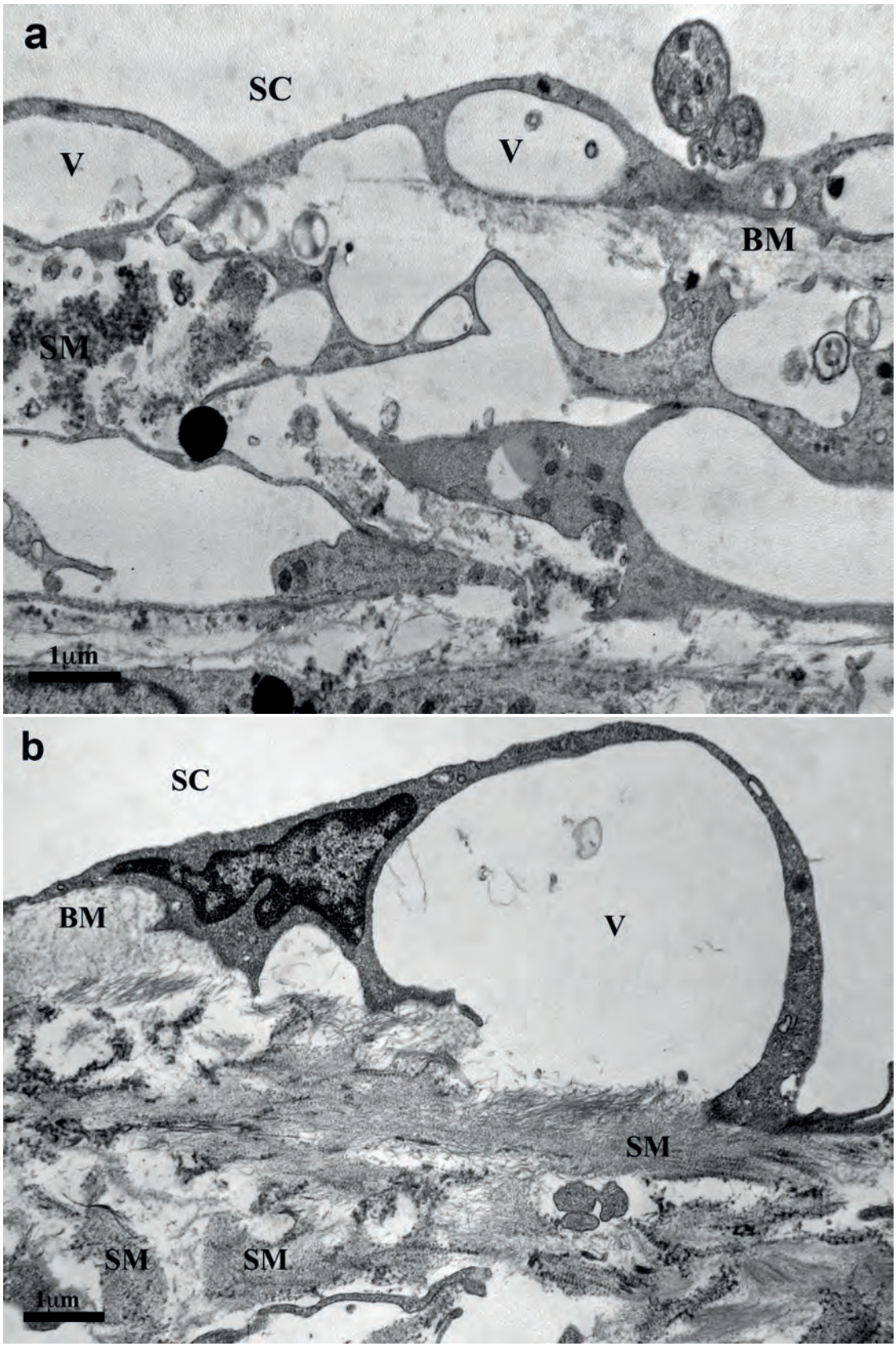

Fig. 5. Increased extracellular matrix in the JCT of POAG eyes. **a.** A transmission electron micrograph of the juxtacanalicular tissue (JCT) region of a normal human eye from a 78-year-old donor. Giant vacuoles (V) are seen along the inner wall of Schlemm's canal (SC). Basement membrane (BM) and sheath material (SM) are seen. **b.** A transmission electron micrograph of the JCT region of a POAG eye from a 92-year-old donor. Compared to the normal eye, significant increases in both BM and SM are seen. (Images provided by Haiyan Gong.)

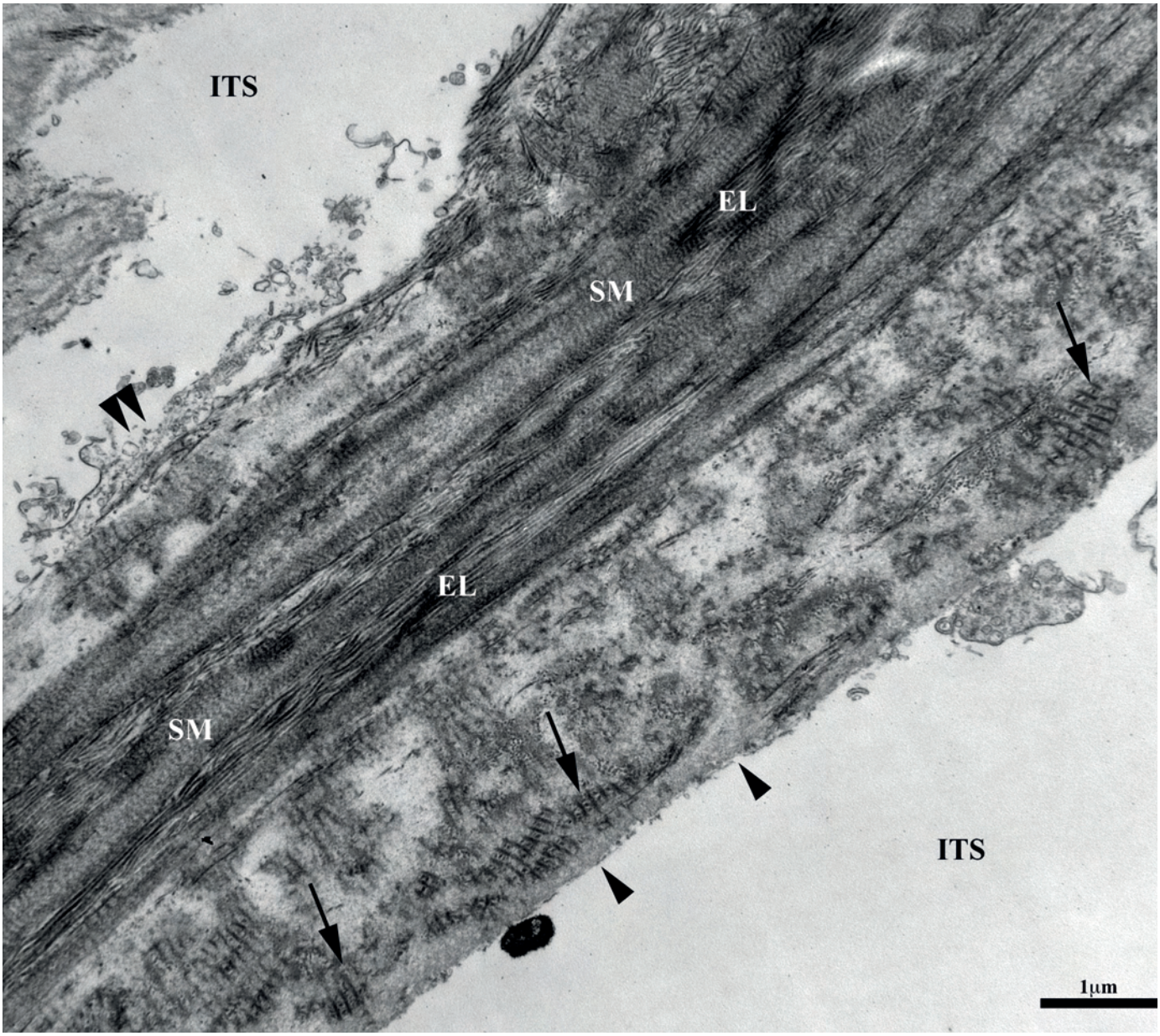

Fig. 6. Cell loss and increased long-spacing collagen in the trabecular beams of a POAG eye. A transmission electron micrograph showing a trabecular beam from an eye with POAG. The endothelial cells that covered the trabecular beam are either gone (arrowheads) or fragments of the cells remain (double arrowheads). The trabecular beam became thicker with increased long-spacing collagen (arrows). EL = elastic fibers; SM = sheath material of elastic fiber; ITS = intertrabecular spaces. (Image provided by Haiyan Gong.)

the scleral spur acts through the 'ciliary muscle-scleral spur-trabecular meshwork' network.[55] Attached to the posterior aspect of the spur, the longitudinal fibers of the ciliary muscle contract to pull on the scleral spur, subsequently pulling and opening up the corneoscleral portion of the TM attached to the anterior aspect of the spur.[56,57] This action facilitates the separation of the trabecular beams to allow more aqueous humor outflow from the anterior chamber.[54,58] One treatment option to decrease IOP has been to target the ciliary muscle with cholinergic agonists, such as pilocarpine. This drug activates the ciliary muscle to contract, opening up the beams of the TM to increase aqueous outflow. Upon loss of attachment of the ciliary muscle, this function of the spur is lost.[59] Additionally, the circumferentially oriented elastic and collagen fibers of the scleral spur give it an increased rigidity compared to the sclera, which allows the spur to support SC.[54,60] The elastic fibers are continuous with those of the trabecular beams and the cribriform plexus of the JCT.[8,54,60,61] When the ciliary muscle contracts, these fibers tense the inner wall of SC and prevent collapse

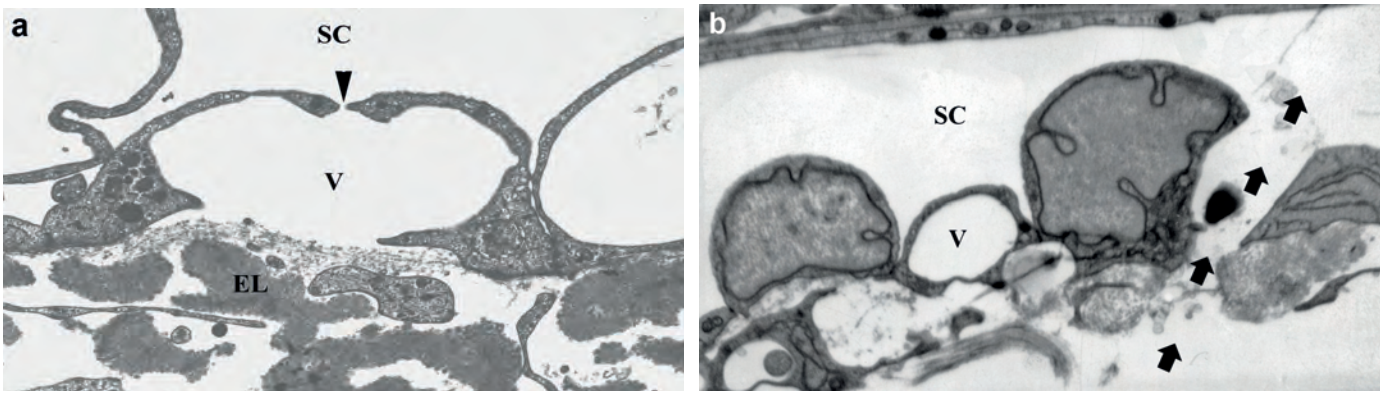

Fig. 7. Giant vacuoles and two types of pores in the inner wall of Schlemm's canal. **a.** The juxtacanalicular tissue region with elastic fibers (EL) and the basement membrane of the inner wall endothelium of Schlemm's canal (SC) with a giant vacuole (V) and an intracellular pore leading into SC (arrowhead) is shown. Aqueous humor is believed to traverse the inner wall of SC though pores. (Image from Gong H, Ruberti J, Overby D, *et al.* A new view of the human trabecular meshwork using quick-freeze, deep-etch electron microscopy. Exp Eye Res 2002; 75:347-358.) **b.** A paracellular pore (B pore) is seen here located at the border between two adjacent endothelial cells. Arrows indicate the direction of the outflow. (Image from Ye W, Gong H, Sit A, Johnson M and Freddo TF. Immersion fixation vs. fixation under flow: A study of changes in the structure of interendothelial junctions of Schlemm's canal in normal human eyes. Invest Ophthalmol Vis Sci 1995;36(suppl):S729.)

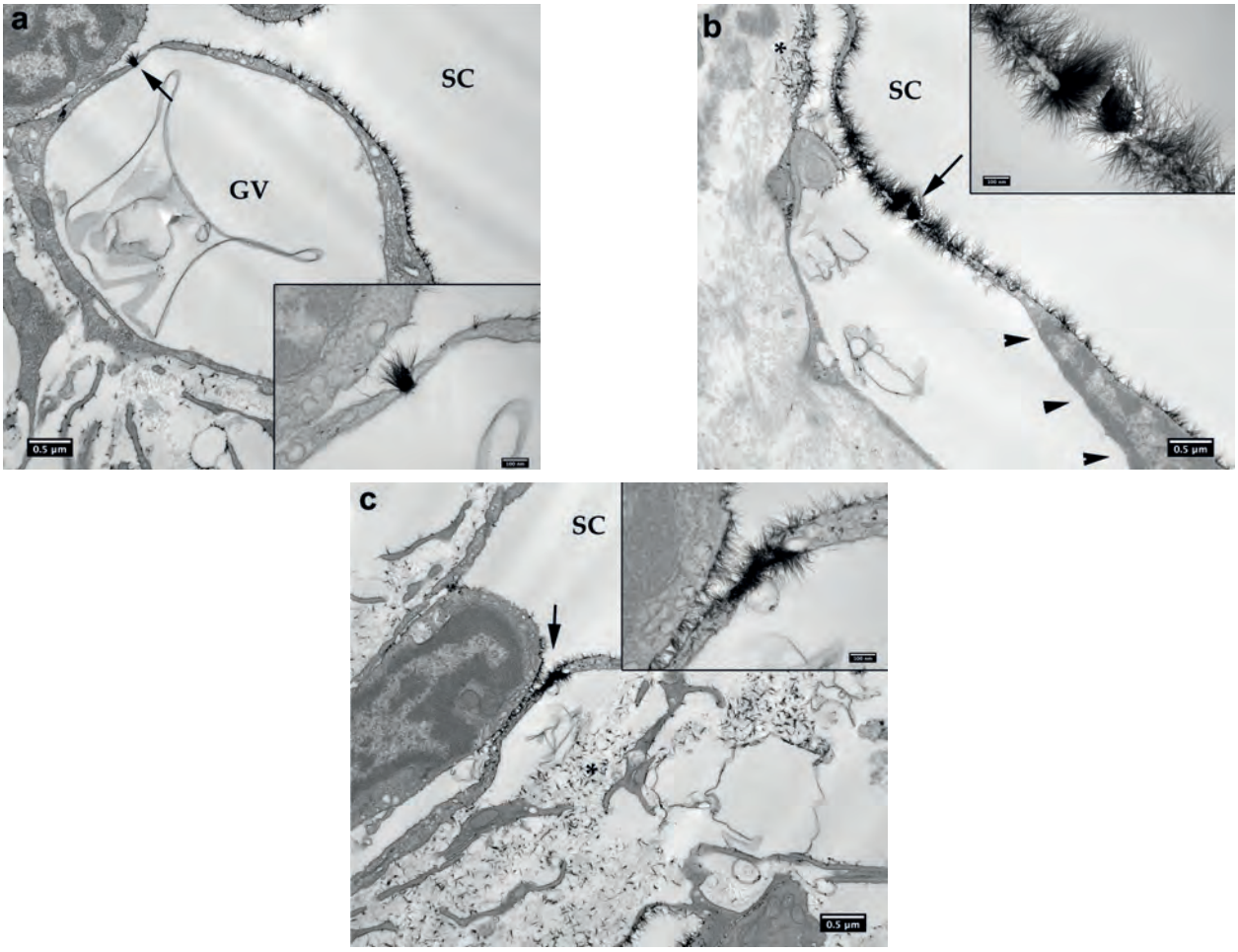

Fig. 8. Pores filled with glycocalyx. **a.** A pore in a giant vacuole (GV) (arrow, insert) of a human eye is filled with glycocalyx, which also coats the outer membrane, but not the inner membrane of the GV; note the membranous material apparently in the passage through the GV. **b.** Glycocalyx was seen within a pore of a giant vacuole (arrow), and coating the outer surface and left side of the inner membrane of the giant vacuole, which is close to a basal opening (*), but not the right side of the inner membrane of the giant vacuole (arrowheads) in a human eye. **c.** Glycocalyx was seen filling a pore not associated with the giant vacuole (arrow). All insets show the pore filled with glycocalyx at a higher magnification. Significant Alcian Blue staining was also seen in the basal side of extracellular matrix (*). (Modified from ref. 45.)

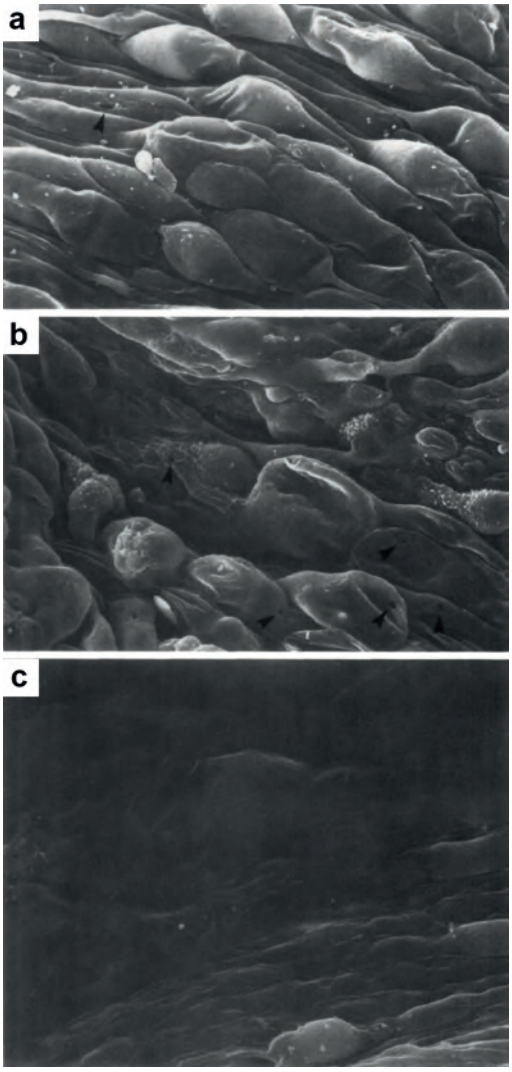

Fig. 9. Scanning electron microscopic (SEM) images of the inner wall endothelial cells in normal and POAG eyes perfused at 15 mmHg. **a.** SEM of the inner wall endothelial lining in a normal eye. A pore (arrow) is observed at the base of a bulging structure. Original magnification X3500. **b.** SEM of the inner wall endothelium in a POAG eye. The appearance of the bulges in the inner wall lining is less uniform. A cluster of pores (arrow) is present. Original magnification X3500. **c.** SEM of the inner wall endothelial lining in a POAG eye depicting an area devoid of bulges and pores. Such flat areas were more commonly seen in POAG eyes than in normal eyes. Original magnification X3100. (Modified from ref. 47.)

under high-pressure conditions.[62,63] In mice, treatment with pilocarpine increases the lumen size of SC when compared to untreated eyes.[63] However, a shorter scleral spur with fewer elastic and collagen fibers may be inadequate to open up the TM and support and prevent collapse of SC.

One initial study by Nesterov *et al.* reported a significantly shorter scleral spur length in POAG eyes compared to normal eyes,[55] and suggested that this short scleral spur could predispose a patient to collapse of SC. A subsequent study by Moses and Arnzen[58] reported a normal length nearly double the value of that reported in the Nesterov study, but they did not examine the length in POAG eyes. A recent study resolved the literature dispute by repeating Nesterov's and Moses's methods and developing a new method of measurement (Fig. 10a, b).[64] This study confirmed the presence of a shorter scleral spur in POAG eyes compared to normal, non-diseased eyes (Fig. 10c). In addition, this study also showed a strong, positive correlation between the scleral spur length and the age at which patients are diagnosed with POAG (Fig. 10d).[64] Using clinical records from the POAG eyes, Swain *et al.* found that patients with longer scleral spurs were diagnosed at later ages, suggesting the scleral spur's significance in regulating aqueous outflow. A shorter scleral spur, having less of the TM inserted into its anterior aspect, would open up fewer beams and produce less tension in the IW of SC, which could fail to increase aqueous outflow, predisposing a patient to developing POAG.[55,58,64,65] If the scleral spur were measureable *in vivo*, its length could potentially be used as a risk factor of POAG.

Grierson *et al.* developed a method[66] to measure the angle between the axis of the scleral spur and the scleral sulcus (Fig. 11a). This study investigated the change in the angle when eyes were treated with pilocarpine to activate the ciliary muscle. Swain *et al.* used this method to examine the difference in resting angle in normal and POAG eyes. The angle in POAG eyes was significantly wider than that in normal eyes, suggesting that upon ciliary muscle contraction, the POAG scleral spur would not be able to move as much to the posterior as a scleral spur in a normal eye (Fig. 11b).[64] Moses and Arnzen[58] developed a mathematical model to measure the effectiveness of the scleral spur in opening up the corneoscleral trabecular beams and supporting SC using the scleral spur length and Grierson angle[66] measurements. This study calculated the theoretical distance (Δh) that the scleral spur would move *in vivo* using measurements taken from cadaver eyes (Fig. 11c). With this model, Moses and Arnzen determined the minimum distance that the scleral spur would need to move to the posterior to change the conformation of the TM, support SC, and allow increased aqueous outflow.[58] Swain *et al.* used Moses's model to compare the effectiveness of the scleral spur in POAG and normal eyes and showed that the mean distance moved by scleral spurs in POAG eyes did not meet the

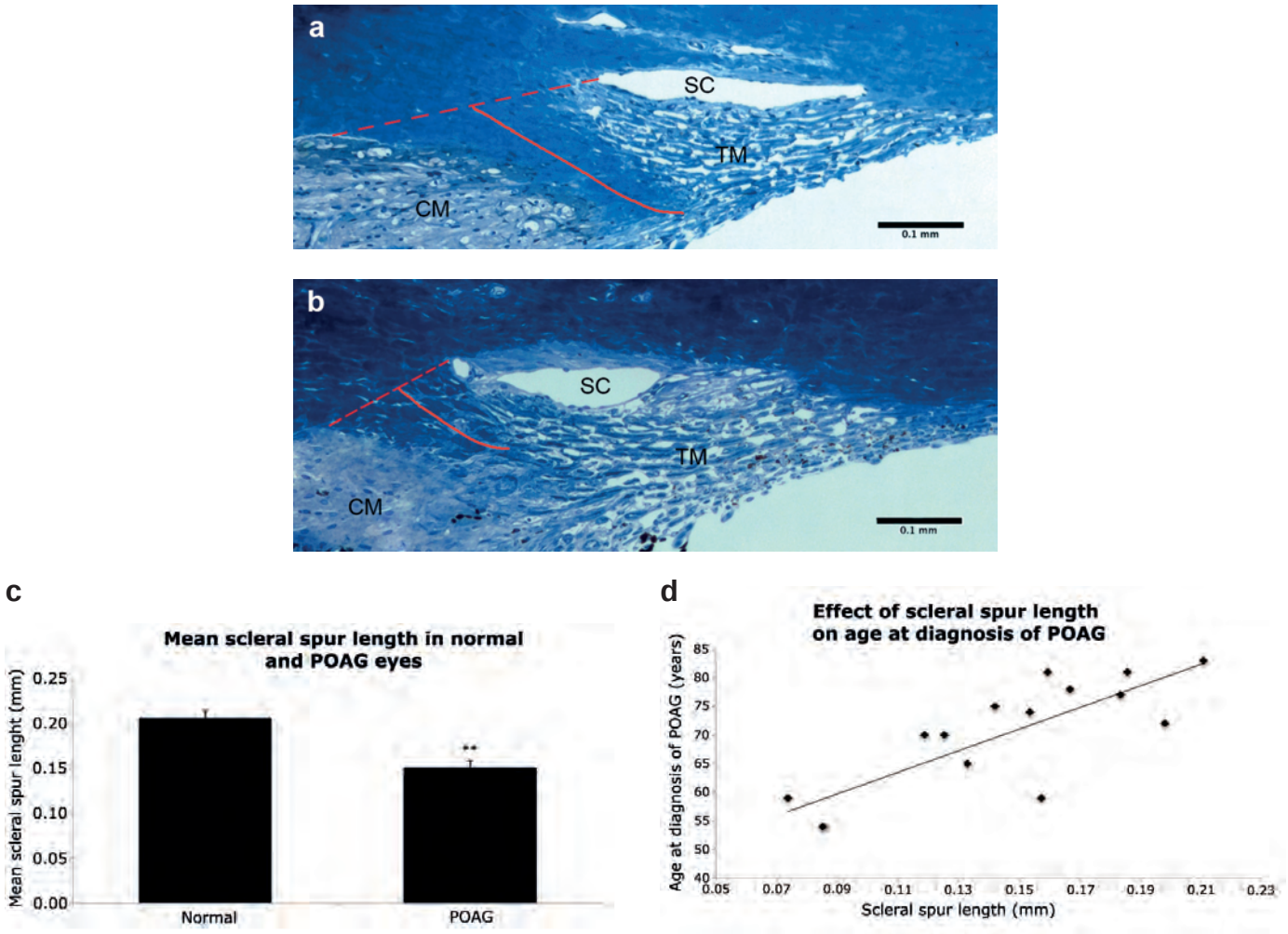

Fig. 10. Shorter scleral spur in the POAG eyes and the relationship between scleral spur length and patient age at diagnosis of POAG. **a-c.** The mean scleral spur length was significantly shorter in POAG eyes than in normal eyes. Error bars = SE; ** = $p \leq 0.001$. The solid line represents scleral spur length, drawn from the tip of the scleral spur to the middle of the red dotted line, which connects the anterior and posterior points where the sclera curves out to form the spur. CM = ciliary muscle, SC = Schlemm's canal, TM = trabecular meshwork. **d.** A significant, positive correlation was observed between scleral spur length (mm) and the patient's age in years at diagnosis of POAG ($p < 0.001$). (Modified from ref. 64.)

minimum required to increase aqueous outflow (Fig. 11d), suggesting that the scleral spur length could determine the efficacy of the 'ciliary muscle-scleral spur-trabecular meshwork' network.[64] Recent studies have investigated the possibility of identifying and measuring the scleral spur *in vivo* using optical coherence tomography.[67-70] If this technology produced images with high enough resolution to measure the scleral spur precisely, the length of the scleral spur could be used as an indicator for a patient's predisposition to develop POAG.

6. The collapse of Schlemm's canal

The anterior to posterior width of SC has been reported as about 300 µm wide with a maximum inner to outer wall height of about 30 µm.[62,64] Increasing IOP leads to the progressive collapse of SC (Fig. 12a, b).[63,71-73] As SC narrows, the outflow resistance grows, and the IOP rises even more.[74,75] This progressive collapse has been reported to be reversible upon lowering IOP back to a normal level in bovine,[76] mouse,[63] and human (Fig. 12c)[77] eyes. Interestingly, a recent study reported that pilocarpine was able to maintain the lumen size of SC by ciliary muscle contraction in mice, even while increasing IOP.[63] In POAG, the dimensions of SC including the height and cross-sectional area are significantly smaller than in healthy eyes (Fig. 12d, e),[64,78,79] a histo-

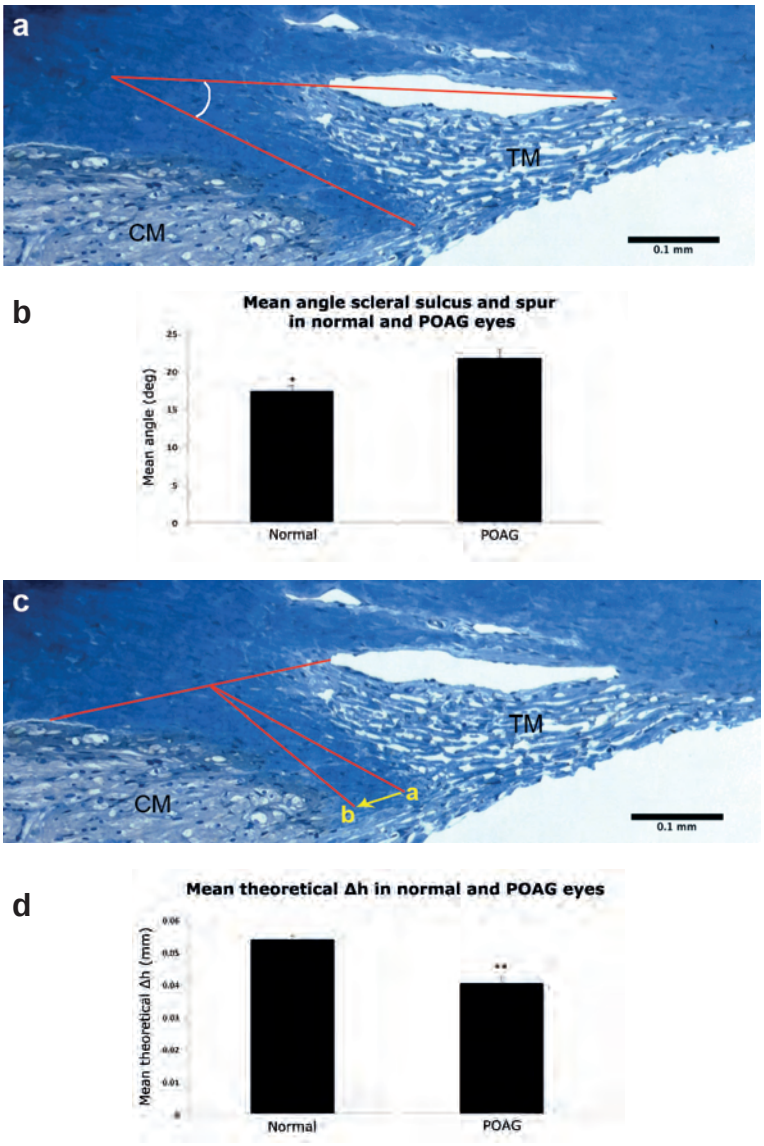

Fig. 11. Comparison of angle between scleral sulcus and spur and analysis of posterior movement of scleral spur upon ciliary muscle contraction in normal and POAG Eyes. **a.** Measurement of the angle between the scleral sulcus and the scleral spur, as outlined in Grierson *et al.* (1978).[66] The curved line indicates the angle measured. **b.** Mean angle was significantly wider in POAG eyes, compared to normal eyes. Error bars = SE; * = $p < 0.05$. **c.** Upon ciliary muscle contraction, the scleral spur moves from point A to point B. A horizontal distance (Δh) of at least 0.047 mm (yellow arrow) is needed to fully open up the TM and support SC to maintain adequate outflow, according to Moses and Arnzen (1980). **d.** The scleral spur in normal eyes would move a distance greater than the required value of 0.047 mm; whereas, the scleral spur in POAG eyes would move a distance less than the required value and significantly shorter than the distance in normal eyes ($p < 0.0001$). Errors bars = SE; ** = $p < 0.0001$. (Modified from ref. 64.)

logical finding recently confirmed by spectral-domain optical coherence tomographic assessment in patients with POAG.[80] Swain *et al.* investigated the frequency of collapse in normal and POAG eyes by measuring the percentage of SC collapse in cadaver eyes (Fig. 13a).[64] This study reported that POAG eyes experience significantly more percent collapse of SC than normal eyes (Fig. 13b). In addition, significantly more collapse of SC was associated with a shorter scleral spur (Fig. 13c),[64] which could compromise the 'ciliary muscle-scleral spur-trabecular meshwork' network that maintains the patency of the lumen of SC. The reduced size or diameter of SC has been shown to account for nearly half of the decrease in outflow facility observed in eyes with POAG.[78] Additionally, SC became smaller after successful filtration surgery, most likely due to under-perfusion of the TM.[81] The decrease in the size of SC after successful filtration surgery could make glaucoma more difficult to control if the filter ultimately fails.

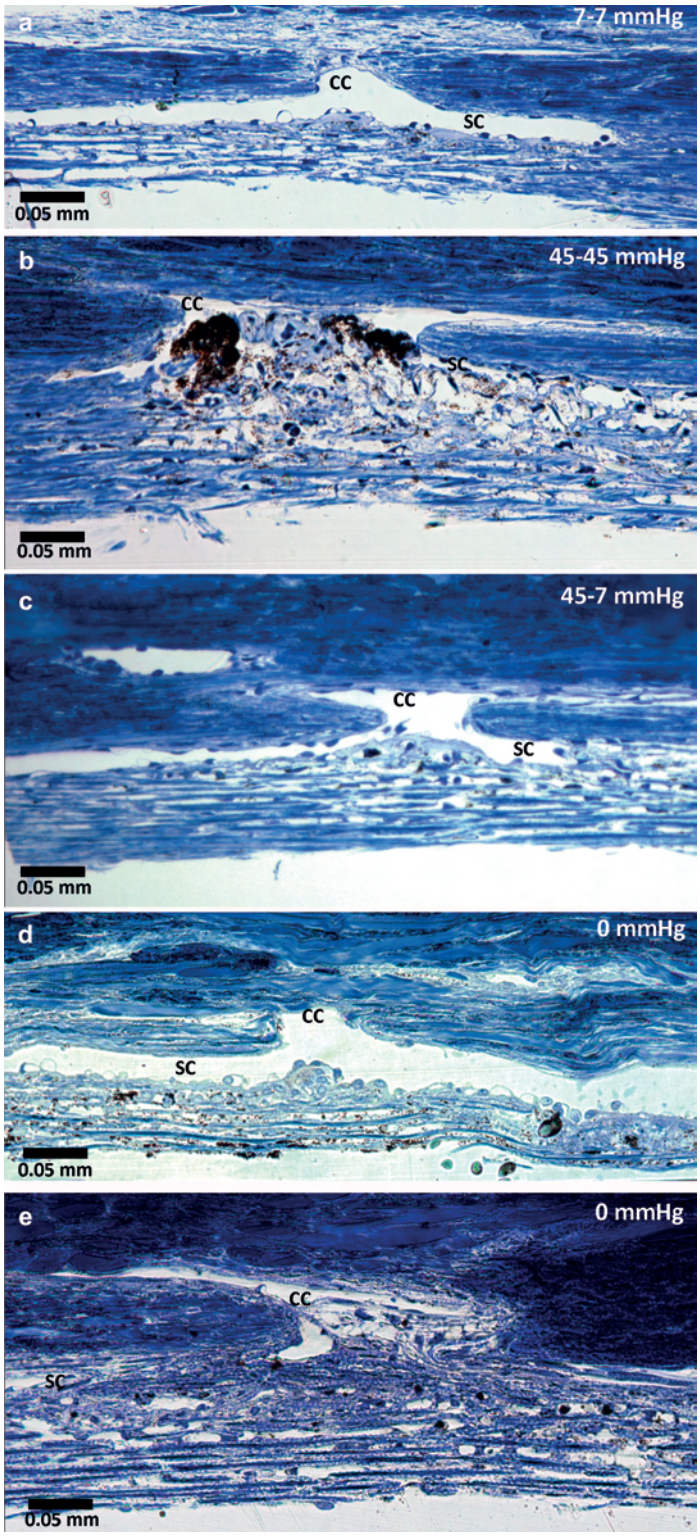

Fig. 12. Collapse of Schlemm's canal and herniation into the collector channel ostia with increased IOP in normal human eyes and in POAG eye. **a.** When a normal human eye was continually perfused at 7 mmHg (normal IOP for a enucleated eye without episcleral venous pressure), Schlemm's canal (SC) was open, and no herniation into the collector channel (CC) ostium was visible. **b.** When the eye was continually perfused at 45 mmHg, SC was collapsed, and the trabecular meshwork was herniated into the CC ostium. **c.** The eye was first perfused at 45 mmHg, followed by a reduction to 7 mmHg. Lowering the pressure reversed the herniation that was seen at 45 mmHg. Only deformation of the trabecular meshwork was seen facing the CC ostium region. SC was wider in this eye than in the one perfused continuously at 45 mmHg (b). **d.** When a normal eye was fixed at 0 mmHg, SC was open and the herniation was not visible at the CC ostium. **e.** In comparison, when an eye with POAG was fixed at 0 mmHg, a collapse of SC adjacent to both sides of CC ostium with focal adhesions between the inner wall and outer wall of SC and herniations of the inner wall and JCT into CC ostia were observed. (From ref. 93.)

7. Herniations block the collector channel ostia

When the IOP rises, the TM extends toward the outer wall of SC and leads to the progressive collapse of SC and increased outflow resistance.[72,73,82,83] Because there is no outer wall of SC in the region of the collector channel (CC) ostia, the JCT and inner-wall tissue herniates into the CC ostia (Fig. 12).[72,84] Under experimental conditions in healthy eyes, the herniations were reversible when the IOP decreased from high to normal levels.[76] Permanent herniations were common among eyes with POAG, even when the eyes were fixed at zero pressure (Fig. 12).[84] In an experimental study, co-localization of tracer and pigment was found in the TM, mostly near CC ostia regions, of healthy enucleated eyes;[85] therefore, pigment can be used as an internal marker for preferential flow. A decrease in pigment was found in the TM herniated into CC ostia, which suggests diminished outflow in these regions.[84] The obstruction of CCs was also detected in patients with POAG through an evaluation of the fluorescein egress from SC to the episcleral veins and blood reflux from the episcleral veins to SC.[77,86] These findings strongly suggest that the obstruction of CCs contributes to increased outflow resistance found in eyes with POAG.

8. The relationship between morphological changes and reduction in active outflow area

Aqueous humor outflow through the trabecular outflow pathway is segmental or circumferentially non-uniform (Fig. 14) based on the observation of the distribution of pigment in the TM,[85] tracer perfused into the anterior chamber of enucleated normal non-human and human eyes,[47,72,85,87-96] and *in vivo* injection of tracer into the anterior chamber of mouse eyes.[97] These results suggest that at any given time, only a fraction of the outflow pathways are actively involved in aqueous humor drainage. A greater concentration of tracer was observed in the TM adjacent to collector channel ostia, but not all the collector channel ostia are active at a given time (Fig. 15).[93,98] The implication of segmental flow is significant, because it confers the existence of circumferential variations of the TM structure, meaning that cells and tissues may respond to drugs at varying

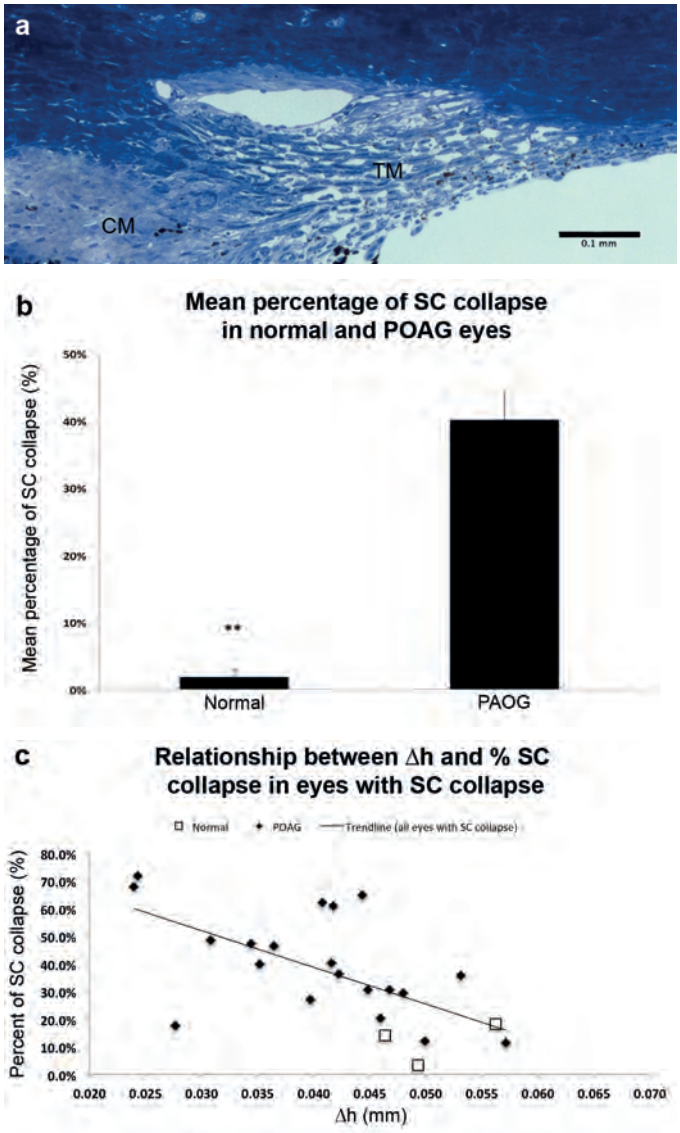

Fig. 13. Collapse of SC in POAG and its relationship with the scleral spur. **a.** Measurement of the percentage of collapse of SC, shown in a POAG eye. The red line represents the length of SC collapse; the green line represents the total length of SC. **b.** Mean percentage of collapse of SC was significantly higher in POAG eyes (40.08 ± 4.13%; mean ± SE) than in normal eyes (1.78 ± 1.12%; $p < 0.0001$). Error bars = SE; ** = $p \leq 0.001$. **c.** Using only eyes that exhibited SC collapse, a significant, negative correlation was observed between the distance of posterior movement (Δh mm) and the percent collapse of SC ($R2 = 0.528$, $n = 23$; $p < 0.001$). (Modified from ref. 64.)

magnitudes, depending on the amount of flow (and therefore, amount of the drug) through that region of the TM. Recent studies have shown the differences in morphology (Fig. 15)[93] and molecular compositions (Fig. 16) between high and low flow regions in the TM and JCT.[91] More expanded (or thicker) TM and JCT regions (Figs. 15, 16), less versican and more type VI collagen were found associated with high flow regions (Fig. 17).[91,92]

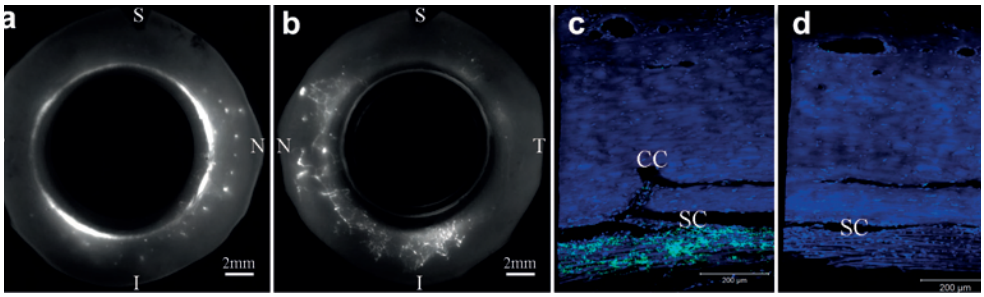

Fig. 14. Segmental aqueous flow pattern in normal human eyes. **a.** Posterior view of the tracer distribution in the trabecular meshwork (TM) in a global image. Segmental tracer distribution is seen. **b.** Segmental tracer distribution is seen in the scleral veins in the anterior view of a global image. **c.** A confocal microscopic image showing more tracer (green) near the collector channel (CC) ostia region. **d.** A confocal microscopic image showing no tracer was seen in this region of the TM. S= superior; N= nasal; I= Inferior; T= temporal. (From ref. 77.)

Active flow area was reduced with acute elevation of IOP in bovine eyes. Outflow patterns in the JCT and inner wall transitioned from less segmental (more uniform) patterns at normal IOP (7 mmHg in enucleated eyes) to an increasingly segmental pattern at higher IOP (15-45 mmHg) (Fig. 18).[72] The structural changes associated with decreased active flow area are collapse of the aqueous plexus (equivalent to SC in human) and herniation of the TM into CC ostia (Fig. 19).[72] This decrease in active flow area is also associated with decreased outflow facility and is reversible when pressure is reduced from a high to normal level.[76] Decreased active flow area was also reported during chronic elevation of IOP in a laser-induced monkey glaucoma model,[99] with a lesser amount or no tracer found in areas of the TM with laser injury, including the CC ostia region (Fig. 20). Moreover, active outflow was found shifted away from areas with laser injury to a small area without it (Fig. 21).[99] Significant reduction of active flow area was also reported in POAG eyes compared to normal eyes in a tracer study.[100] More continuous and thicker basement membranes observed along the inner wall of SC, increased ECM deposition in the JCT, and obstruction of the CC ostia by herniations might contribute to the reduction in active outflow areas and outflow facility in POAG. In addition, an inverse correlation between active flow area and IOP was recently documented in an ocular hypotensive mouse model.[97] Collectively, these results suggest that increasing active flow area could be used as a new therapeutic strategy to lower IOP in POAG, which was supported by recent studies using both drugs (such as rho kinase inhibitor, Y-27632[93,98] and new surgical devices (such as the HydrusTM implant[101]) to decrease outflow resistance and thus IOP through increasing active flow area.

9. Summary

This chapter summarizes the histopathological changes found in the trabecular outflow pathway that likely contribute to increased outflow resistance in the eyes with POAG in part through reduction of active flow area. Some of the changes are secondary to the elevation in IOP, but all of them are likely to contribute to the pathogenesis of POAG to some extent. Understanding the mechanism of these histological changes in POAG may provide new insight to develop new therapeutic targets to lower IOP in POAG. In addition, it is possible, in the future, that some of the structural changes in the aqueous outflow pathway, currently being observed only histologically, could be evaluated *in vivo* by OCT or other advanced imaging techniques. In this way, a more personalized treatment plan could be developed if a shorter scleral spur could be identified and/or the site(s) of blockage in the aqueous outflow pathway could be located in each patient.

10. Acknowledgements

The original work reported in this chapter was supported in part by NEI EY-022634, EY-018712, EY-019696 and the Massachusetts Lions Eye Research Fund.

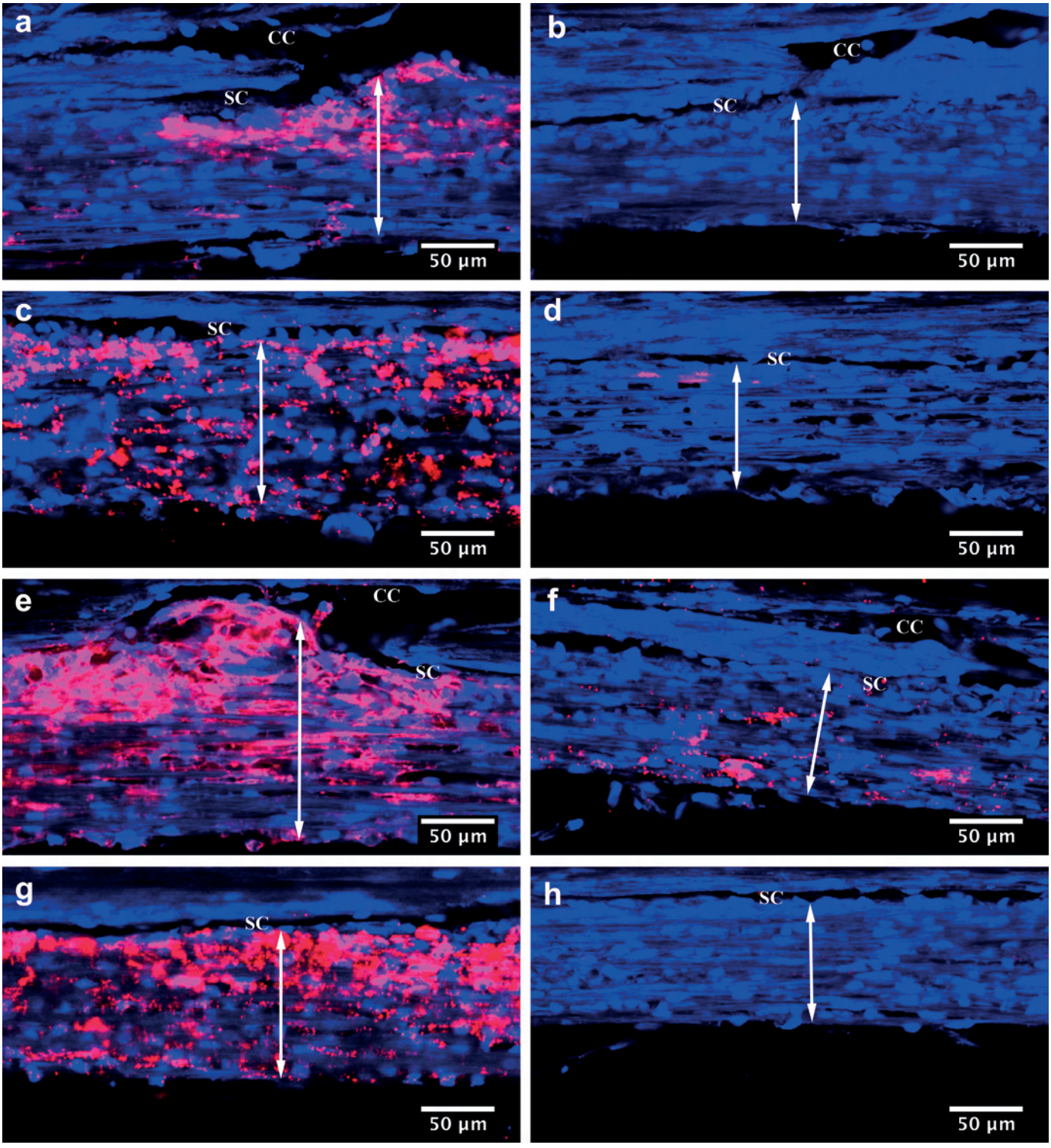

Fig. 15. Difference in TM thickness in the high and low flow regions in normal control and Y27632-treated human eyes. Aqueous outflow pattern through the trabecular meshwork (TM) region with or without collector channel (CC) in Y27632-treated and control eyes. Segmental distribution of fluorescent tracer was observed along the SC in both control **(a-d)** and Y27632-treated eyes **(e-g)**. An increased TM thickness (double arrow) was found in the high-tracer region **(a, c, e, g)** compared to the low-tracer region **(b, d, f, h)**. More fluorescent tracers were found near some CC ostia **(a, e)** but not the other regions near CC ostia **(b, f)**. (From ref. 93.)

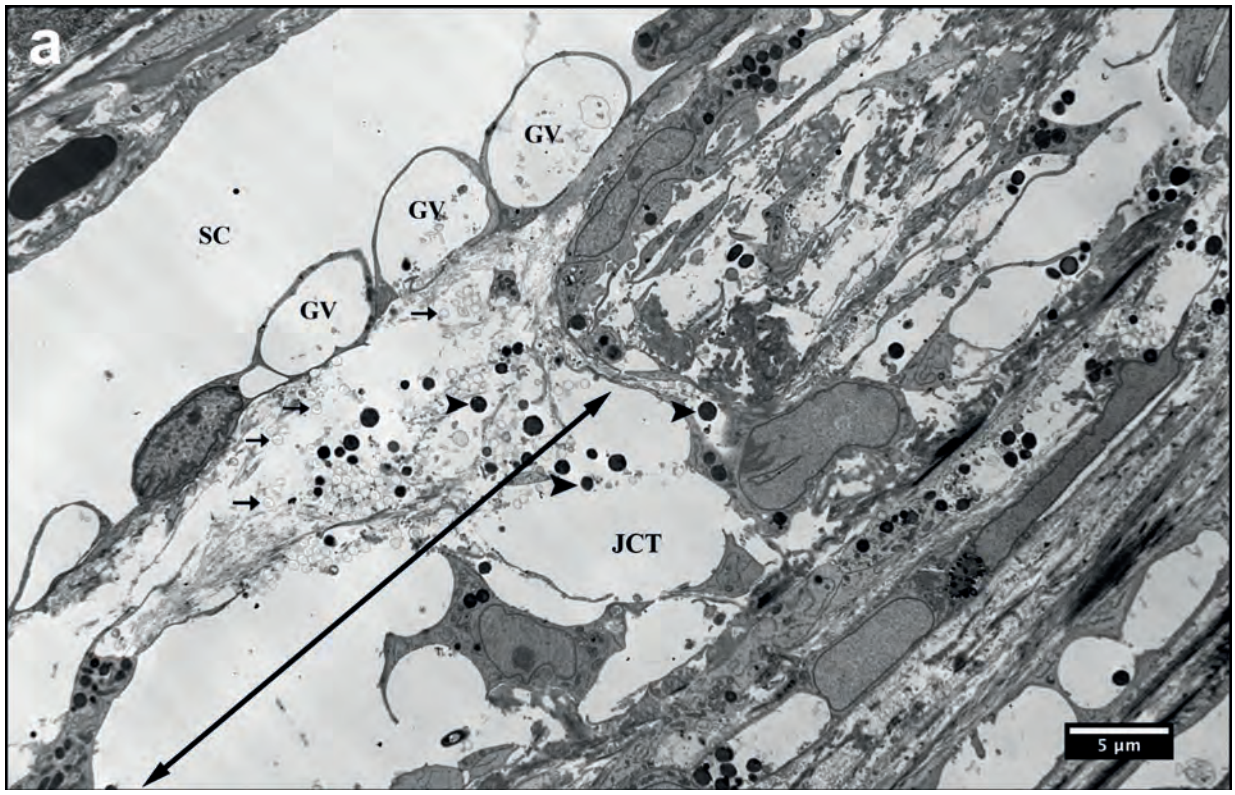

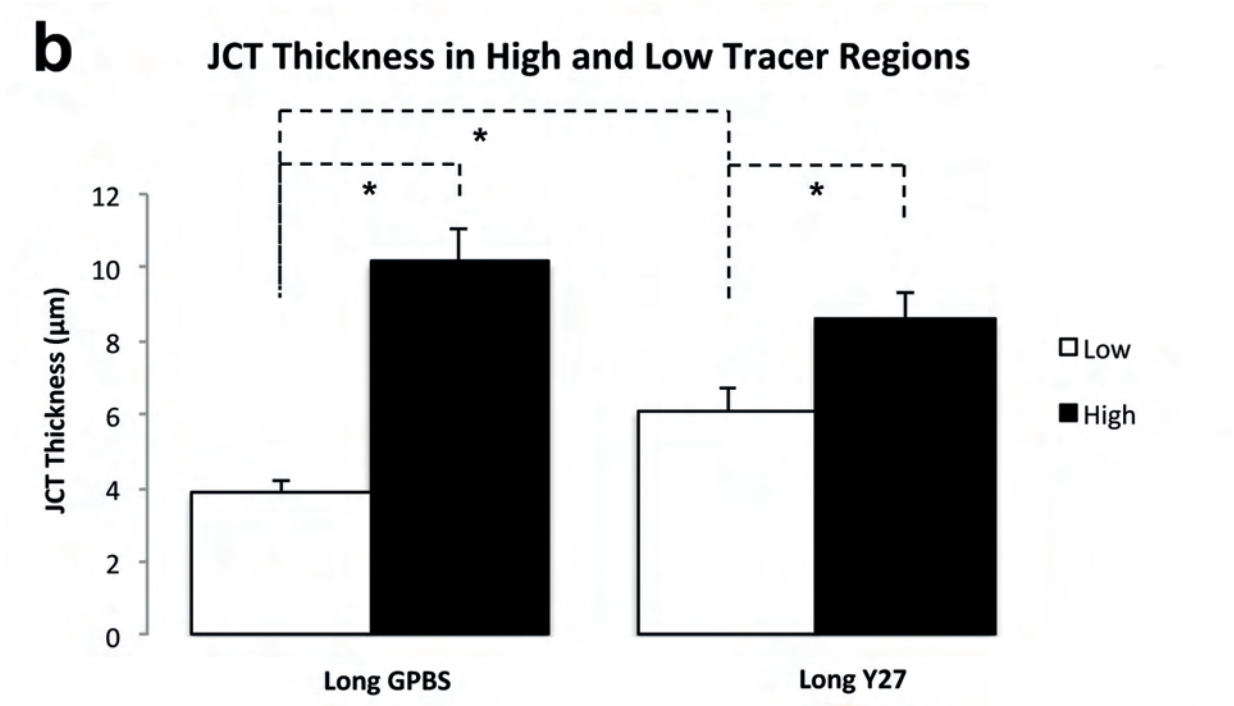

Fig. 16. Electron microscopic analysis of high and low flow region in the JCT. **a.** Fluorescent microspheres (arrows) and pigments (arrowheads) were seen in the loose JCT region, which contains larger optical empty space (double arrow) than dense JCT (non-double arrow). No fluorescent microspheres were seen in the giant vacuoles (GV). SC = Schlemm's canal; JCT= Juxtacanalicular connective tissue. **b.** JCT thickness in high and low tracer regions. High-tracer regions had significantly higher JCT thickness compared to low-tracer regions in both long-duration Y27632 and GPBS groups ($p < 0.05$). Y27632 group had significantly higher JCT thickness compared to GPBS group at low-tracer regions ($p < 0.01$), while no difference was found at high-tracer regions. (From ref. 93.)

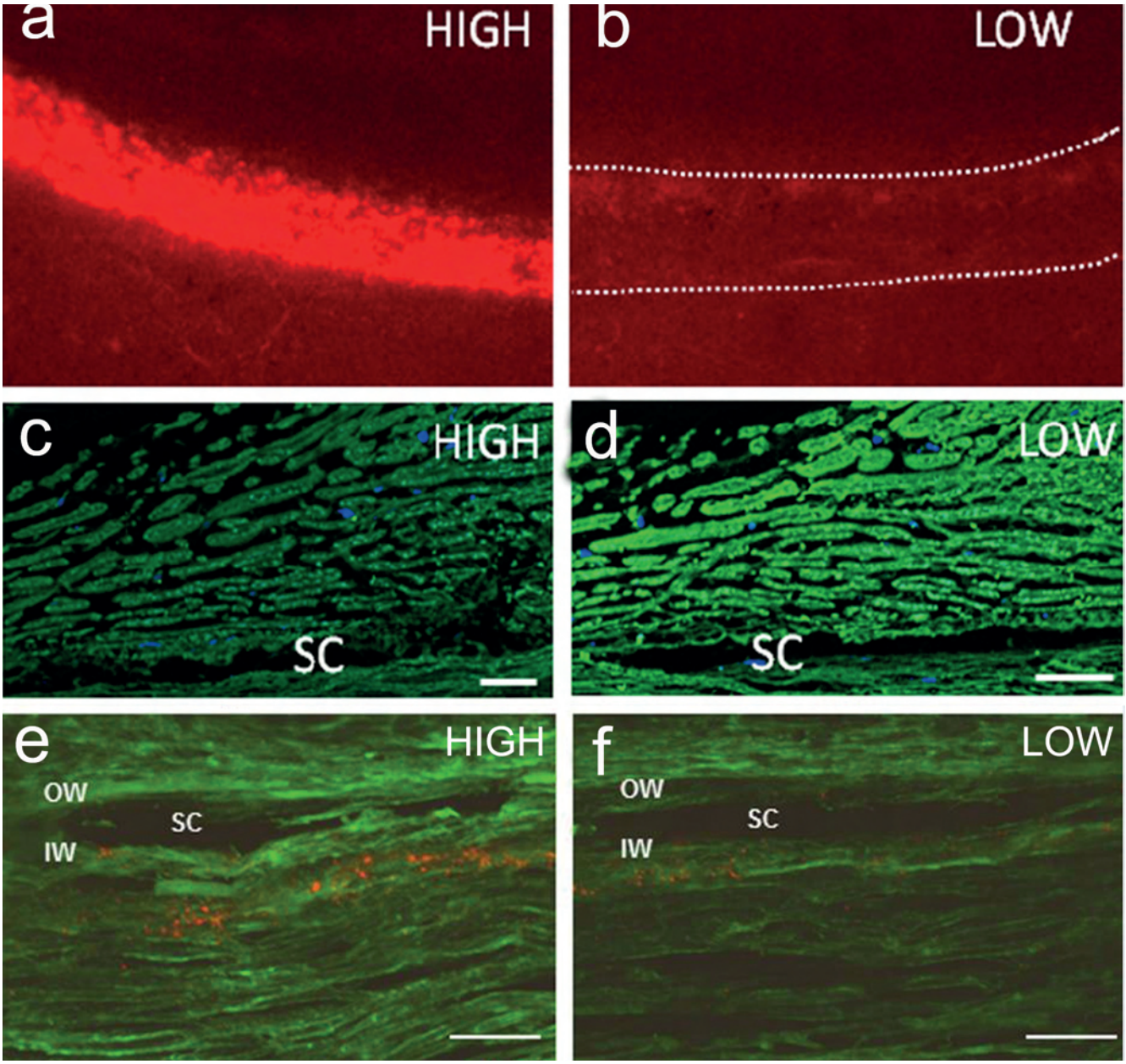

Fig. 17. Less Versican and more Type VI collagen found in high flow region (a, c) than low flow region (b, d) of human anterior segments. **a.** High flow region with high Qdot labeling (red). **b.** Low flow region with low Qdot labeling. **c-d.** Versican immunostaining (green) in paraffin-embedded radial sections shows less abundant in areas of high Qdot labeling region (c) than low Qdot labeling region (d) in the TM. Images shown were obtained with identical image-acquisition settings on the confocal microscope. SC = Schlemm's canal. Scale bars: (c,d) 20 µm. (Modified from ref. 91.) **e-f.** Stronger immunostaining for Type VI collagen was seen in high flow region (e) than low flow region (f) of the frontal section of TM. Scale bars = 50 µm. OW = Outer wall, SC = Schlemm's canal, IW = Inner wall. (Modified from ref. 92.)

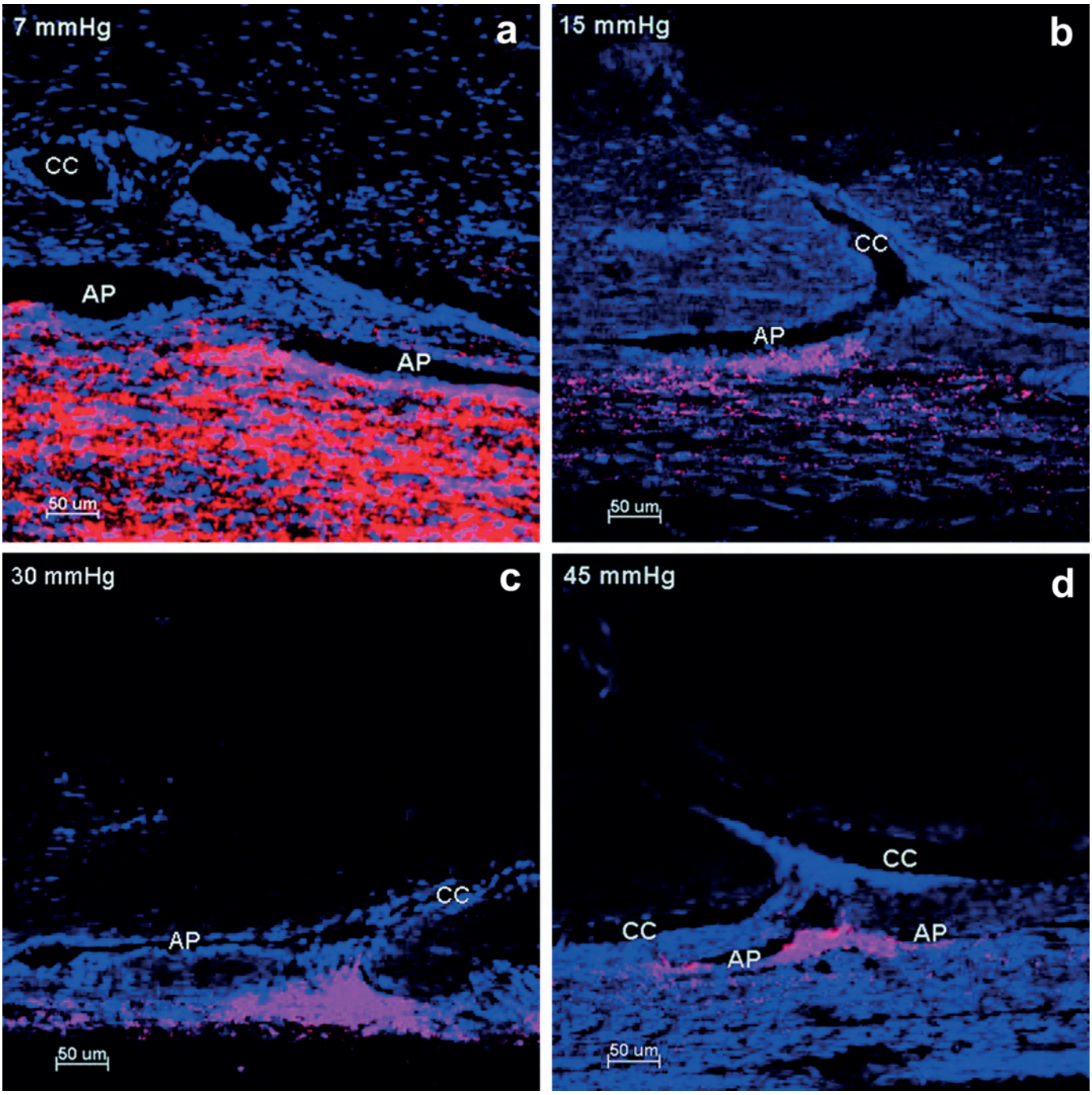

Fig. 18. Confocal microscopy of fluorescent microspheres perfused at four different IOPs in bovine eyes. **a.** At 7 mmHg, a uniform distribution of microspheres (red) was seen along the inner wall of the aqueous plexus (AP). In contrast, at pressures of 15 mmHg **(b)**, 30 mmHg **(c)** and 45 mmHg **(d)** there was a segmental pattern of microsphere distribution with a greater concentration of microspheres in the trabecular meshwork near the collector channel (CC) ostia. This concentrated distribution was visually more dramatic at 45 mmHg than at 15 mmHg. Scale bar = 50 μm. (Image from ref. 72.)

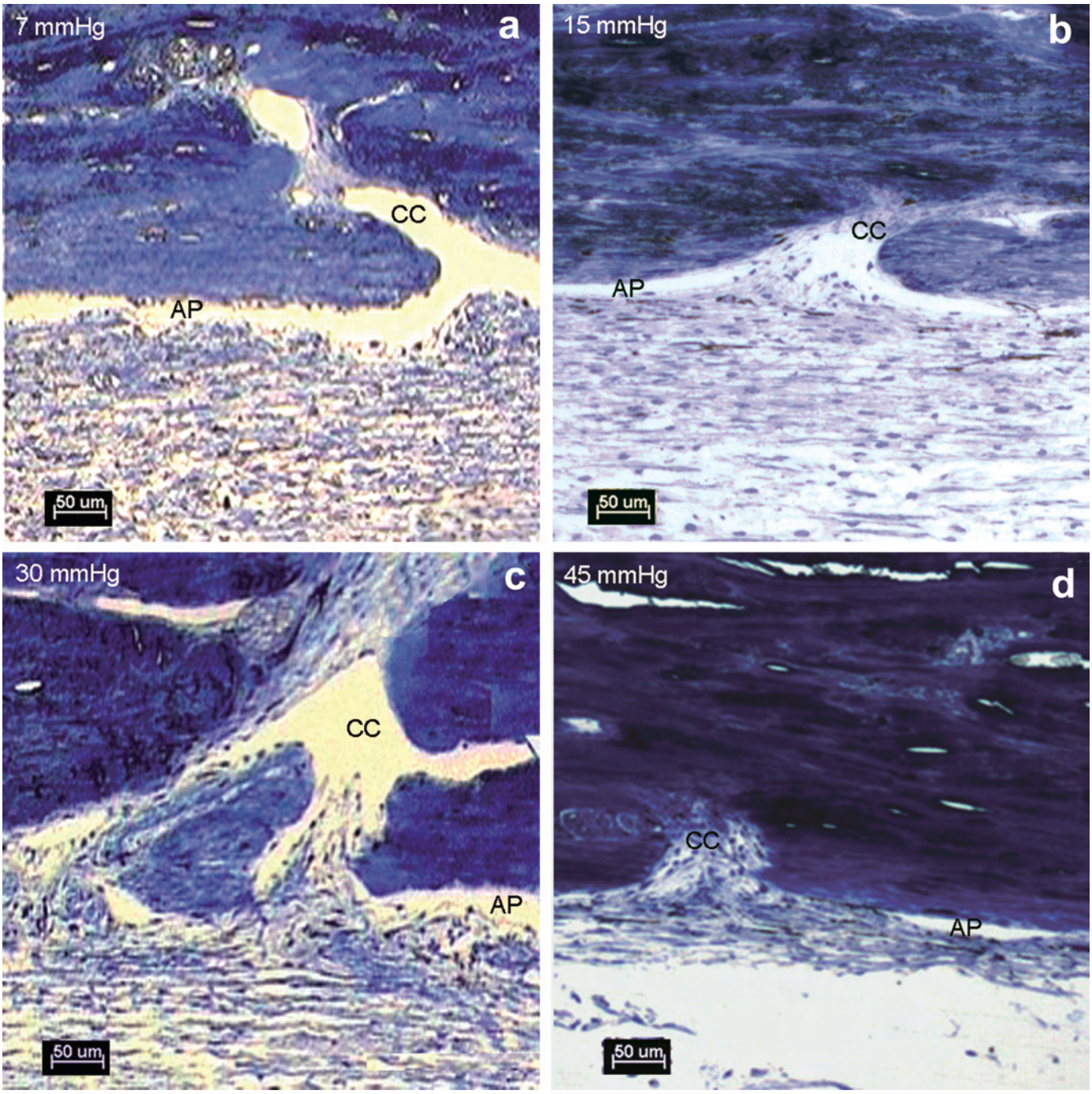

Fig. 19. Light microscopy of the aqueous plexus and collector channels at four different IOPs in bovine eyes. At 7 mmHg **(a)**, the aqueous plexus (AP) was more open compared to the tissue perfused at higher pressures. At 15 mmHg **(b)**, the inner wall and juxtacanalicular tissue (JCT) were partially herniated into the collector channel (CC) ostia. At 30 mmHg **(c)** and 45 mmHg **(d)** the aqueous plexus was collapsed adjacent to the CC ostia. At higher IOP there was a more dramatic herniation of the inner wall and JCT into the CC ostia. Scale bar = 50 µm. (Image from ref. 72.)

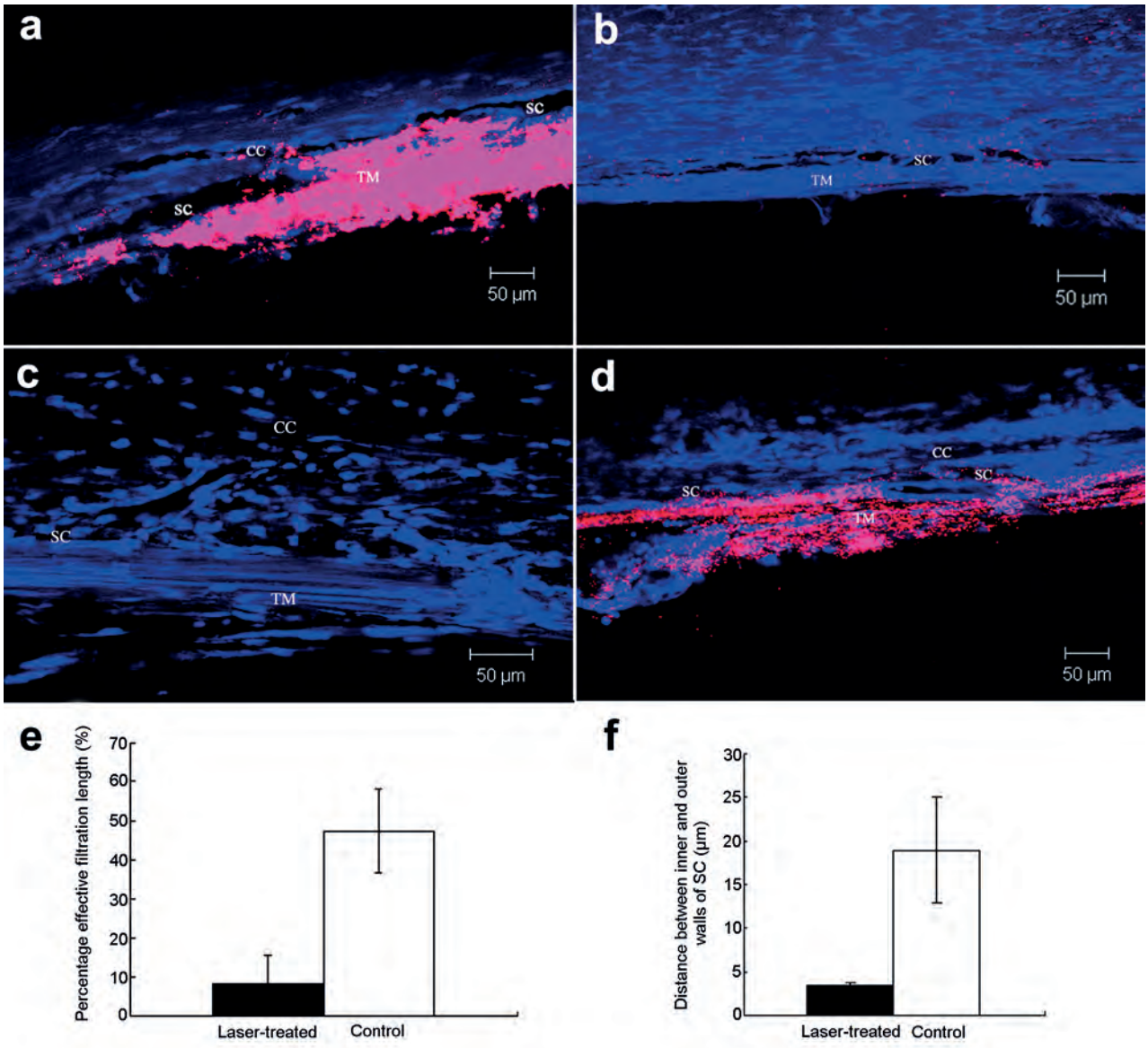

Fig. 20. Comparison of effective filtration length and width of SC in control and laser-induced-glaucoma monkey eyes. **a.** In control eyes, Schlemm's canal (SC) was open and a segmental distribution of microspheres (pink) was found with a greater concentration in the trabecular meshwork (TM) near the collector channel (CC) ostium. **b.** In the lasered region of laser-treated eyes, SC was collapsed and fewer or no microspheres were found in most areas of the TM. **c.** In the lasered region of laser-treated eyes, no microspheres were found in the CC ostium region. **d.** In the non-lasered region of laser treated eyes, a large amount of microspheres (pink) was seen near CC ostia. **e.** The average percent effective filtration length (PEFL = L/TL) in control eyes (47.47 ± 10.79%) was 6-fold larger than in laser-treated eyes (8.40 ± 4.81%, p = 0.013). **f.** The mean distance between the inner and outer wall of SC of control eyes (18.99 ± 6.03 µm) was five-fold greater than laser-treated eyes (3.47 ± 0.33µm, p = 0.01). (Modified from ref. 99.)

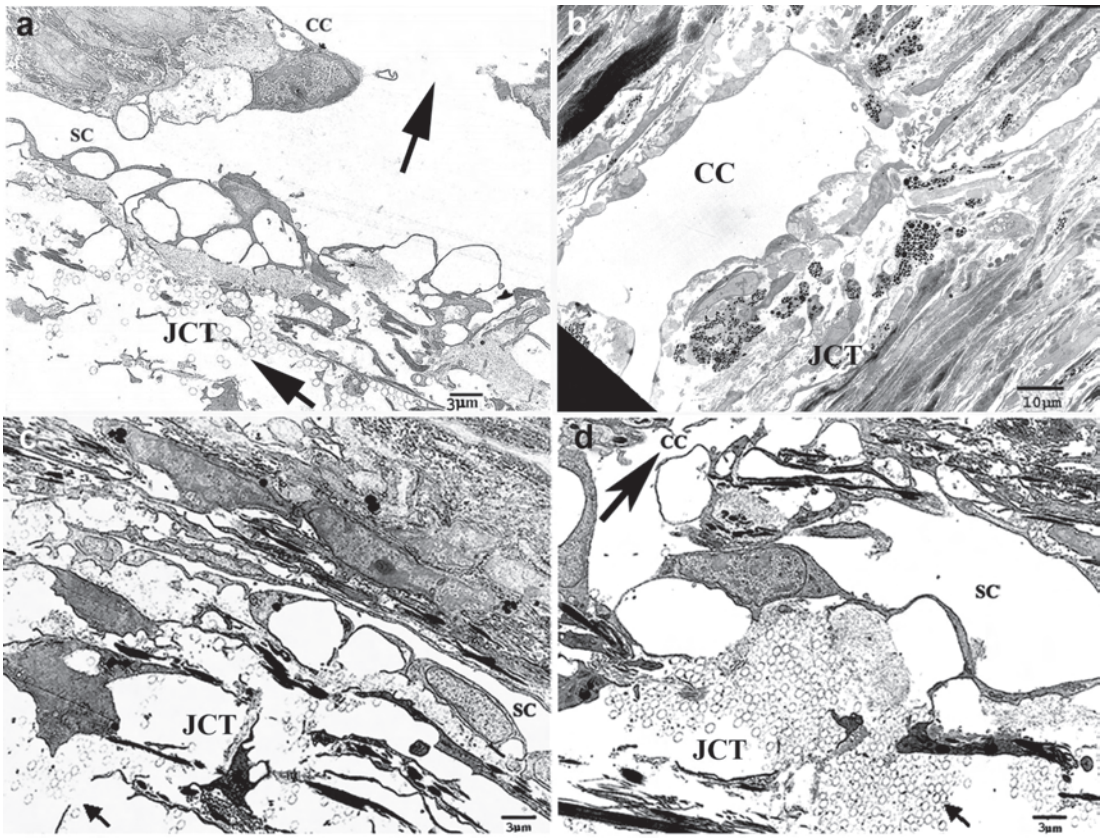

Fig. 21. Electron microscopic analysis of the JCT region in control and laser-induced-glaucoma monkey eyes. **a.** In a normal control eye, numerous giant vacuoles were seen along the inner wall of Schlemm's canal (SC). A greater concentration of microspheres (small arrow) was found in the juxtacanalicular connective tissue (JCT) facing a collector channel (CC) ostium (large arrow). **b.** In a lasered region of a laser-induced glaucoma eye, the JCT and inner wall were herniated into the CC ostium. Pigmentation was found in the JCT cells. The JCT became dense with an increased amount of extracellular matrix material. No microspheres were seen. **c.** In non-lasered areas of a laser-induced glaucoma eye, SC was collapsed. Microspheres (small arrow) were found in the JCT where the extracellular matrix was expanded and looser compared to that in the lasered area (b). **d.** In non-lasered areas of a laser-induced glaucoma eye, more numerous microspheres (small arrow) than that in normal control eyes (a) were found underneath giant vacuoles in the JCT facing a CC ostium (large arrow) where the JCT was more expanded towards a CC ostium. (Modified from ref. 99.)

References

1. Nemesure B, Honkanen R, Hennis A, Wu SY, Leske MC, Group BES. Incident open-angle glaucoma and intraocular pressure. Ophthalmology 2007;114:1810-1815.
2. Grant WM. Experimental aqueous perfusion in enucleated human eyes. Arch Ophthalmol 1963;69:783-801.
3. Bill A, Hellsing K. Production and drainage of aqueous humor in the cynomolgus monkey (Macaca irus). Invest Ophthalmol 1965;4:920-926.
4. Bill A. The aqueous humor drainage mechanism in the cynomolgus monkey (Macaca irus) with evidence for unconventional routes. Invest Ophthalmol 1965;4:911-919.
5. Toris CB, Yablonski ME, Wang YL, Camras CB. Aqueous humor dynamics in the aging human eye. Am J Ophthalmol 1999;127:407-412.
6. Lütjen-Drecoll E, Rittig M, Rauterberg J, Jander R, Mollenhauer J. Immunomicroscopical study of type VI collagen in the trabecular meshwork of normal and glaucomatous eyes. Exp Eye Res 1989;48:139-147.
7. Lütjen-Drecoll E, Rohen JW. Morphology of aqueous outflow pathways in normal and glaucomatous eyes. In: Ritch R, Shields MB, Krupin T (eds), The Glaucomas. St. Louis: Mosby-Year Book, Inc.; 1996:89-124.
8. Lütjen-Drecoll E. Functional morphology of the trabecular meshwork in primate eyes. Prog Retin Eye Res 1999;18:91-119.
9. Acott TS, Kelley MJ. Extracellular matrix in the trabecular meshwork. Exp Eye Res 2008;86:543-561.
10. Borrás T. Gene expression in the trabecular meshwork and the influence of intraocular pressure. Prog Retin Eye Res 2003;22:435-463.
11. Keller KE, Aga M, Bradley JM, Kelley MJ, Acott TS. Extracellular matrix turnover and outflow resistance. Exp Eye Res 2009;88:676-682.
12. Rohen JW, van der Zypen E. The phagocytic activity of the trabecularmeshwork endothelium. An electron-microscopic study of the vervet (Cercopithecus aethiops). Albrecht Von Graefes Arch Klin Exp Ophthalmol 1968;175:143-160.

13. Grierson I, Howes RC. Age-related depletion of the cell population in the human trabecular meshwork. Eye (Lond) 1987;1(Pt 2):204-210.
14. Buller C, Johnson DH, Tschumper RC. Human trabecular meshwork phagocytosis. Observations in an organ culture system. Invest Ophthalmol Vis Sci 1990;31:2156-2163.
15. Alvarado J, Murphy C, Polansky J, Juster R. Age-related changes in trabecular meshwork cellularity. Invest Ophthalmol Vis Sci 1981;21:714-727.
16. Alvarado J, Murphy C, Juster R. Trabecular meshwork cellularity in primary open-angle glaucoma and nonglaucomatous normals. Ophthalmology 1984;91:564-579.
17. Baleriola J, García-Feijoo J, Martínez-de-la-Casa JM, et al. Apoptosis in the trabecular meshwork of glaucomatous patients. Mol Vis 2008;14:1513-1516.
18. Last JA, Pan T, Ding Y, et al. Elastic modulus determination of normal and glaucomatous human trabecular meshwork. Invest Ophthalmol Vis Sci 2011;52:2147-2152.
19. Camras LJ, Stamer WD, Epstein D, Gonzalez P, Yuan F. Circumferential tensile stiffness of glaucomatous trabecular meshwork. Invest Ophthalmol Vis Sci 2014;55:814-823.
20. Morgan JT, Raghunathan VK, Chang YR, Murphy CJ, Russell P. The intrinsic stiffness of human trabecular meshwork cells increases with senescence. Oncotarget 2015;6:15362-15374.
21. Kelley MJ, Rose AY, Keller KE, Hessle H, Samples JR, Acott TS. Stem cells in the trabecular meshwork: present and future promises. Exp Eye Res 2009;88:747-751.
22. Du Y, Roh DS, Mann MM, Funderburgh ML, Funderburgh JL, Schuman JS. Multipotent stem cells from trabecular meshwork become phagocytic TM cells. Invest Ophthalmol Vis Sci 2012;53:1566-1575.
23. Abu-Hassan DW, Li X, Ryan EI, Acott TS, Kelley MJ. Induced pluripotent stem cells restore function in a human cell loss model of open-angle glaucoma. Stem Cells 2015;33:751-761.
24. Yun H, Lathrop KL, Yang E, et al. A laser-induced mouse model with long-term intraocular pressure elevation. PLoS One 2014;9:e107446.
25. Du Y, Yun H, Yang E, Schuman JS. Stem cells from trabecular meshwork home to TM tissue in vivo. Invest Ophthalmol Vis Sci 2013;54:1450-1459.
26. Alvarado JA, Yun AJ, Murphy CG. Juxtacanalicular tissue in primary open-angle glaucoma and in nonglaucomatous normals. Arch Ophthalmol 1986;104:1517-1528.
27. Rohen JW, Lütjen-Drecoll E, Flügel C, Meyer M, Grierson I. Ultrastructure of the trabecular meshwork in untreated cases of primary open-angle glaucoma (POAG). Exp Eye Res 1993;56:683-692.
28. Lütjen-Drecoll E, Shimizu T, Rohrbach M, Rohen JW. Quantitative analysis of 'plaque material' in the inner- and outer wall of Schlemm's canal in normal- and glaucomatous eyes. Exp Eye Res 1986;42:443-455.
29. Gottanka J, Johnson DH, Martus P, Lütjen-Drecoll E. Severity of optic nerve damage in eyes with POAG is correlated with changes in the trabecular meshwork. J Glaucoma 1997;6:123-132.
30. Tripathi RC, Li J, Chan WF, Tripathi BJ. Aqueous humor in glaucomatous eyes contains an increased level of TGF-beta 2. Exp Eye Res 1994;59:723-727.
31. Inatani M, Tanihara H, Katsuta H, Honjo M, Kido N, Honda Y. Transforming growth factor-beta 2 levels in aqueous humor of glaucomatous eyes. Graefes Arch Clin Exp Ophthalmol 2001;239:109-113.
32. Min SH, Lee TI, Chung YS, Kim HK. Transforming growth factor-beta levels in human aqueous humor of glaucomatous, diabetic and uveitic eyes. Korean J Ophthalmol 2006;20:162-165.
33. Ochiai Y, Ochiai H. Higher concentration of transforming growth factor-beta in aqueous humor of glaucomatous eyes and diabetic eyes. Jpn J Ophthalmol 2002;46:249-253.
34. Picht G, Welge-Luessen U, Grehn F, Lütjen-Drecoll E. Transforming growth factor beta 2 levels in the aqueous humor in different types of glaucoma and the relation to filtering bleb development. Graefes Arch Clin Exp Ophthalmol 2001;239:199-207.
35. Lütjen-Drecoll E. Morphological changes in glaucomatous eyes and the role of TGFbeta2 for the pathogenesis of the disease. Exp Eye Res 2005;81:1-4.
36. Welge-Lüssen U, May CA, Lütjen-Drecoll E. Induction of tissue transglutaminase in the trabecular meshwork by TGF-beta1 and TGF-beta2. Invest Ophthalmol Vis Sci 2000;41:2229-2238.
37. Fuchshofer R, Welge-Lussen U, Lütjen-Drecoll E. The effect of TGF-beta2 on human trabecular meshwork extracellular proteolytic system. Exp Eye Res 2003;77:757-765.
38. Neumann C, Yu A, Welge-Lüssen U, Lütjen-Drecoll E, Birke M. The effect of TGF-beta2 on elastin, type VI collagen, and components of the proteolytic degradation system in human optic nerve astrocytes. Invest Ophthalmol Vis Sci 2008;49:1464-1472.
39. Fuchshofer R, Tamm ER. Modulation of extracellular matrix turnover in the trabecular meshwork. Exp Eye Res 2009;88:683-688.
40. Ten Hulzen RD, Johnson DH. Effect of fixation pressure on juxtacanalicular tissue and Schlemm's canal. Invest Ophthalmol Vis Sci 1996;37:114-124.
41. Parc CE, Johnson DH, Brilakis HS. Giant vacuoles are found preferentially near collector channels. Invest Ophthalmol Vis Sci 2000;41:2984-2990.
42. Tripathi R, Tripathi B. Functional anatomy of the anterior chamber of the angle. In: Duane TD, Jaeger EA (eds), Biomedical foundations of ophthalmology: Harper & Row; 1982.
43. Ethier CR, Coloma FM, Sit AJ, Johnson M. Two pore types in the inner-wall endothelium of Schlemm's canal. Invest Ophthalmol Vis Sci 1998;39:2041-2048.
44. Bill A, Svedbergh B. Scanning electron microscopic studies of the trabecular meshwork and the canal of Schlemm--an attempt to localize the main resistance to outflow of aqueous humor in man. Acta Ophthalmol (Copenh) 1972;50:295-320.
45. Yang CY, Huynh T, Johnson M, Gong H. Endothelial glycocalyx layer in the aqueous outflow pathway of bovine and human eyes. Exp Eye Res 2014;128:27-33.
46. Tripathi RC. Aqueous outflow pathway in normal and glaucomatous eyes. Br J Ophthalmol 1972;56:157-174.
47. Allingham RR, de Kater AW, Ethier CR, Anderson PJ, Hertzmark E, Epstein DL. The relationship between pore density and outflow facility in human eyes. Invest Ophthalmol Vis Sci 1992;33:1661-1669.

48. Johnson M, Chan D, Read AT, Christensen C, Sit A, Ethier CR. The pore density in the inner wall endothelium of Schlemm's canal of glaucomatous eyes. Invest Ophthalmol Vis Sci 2002;43:2950-2955.
49. Ainsworth JR, Lee WR. Effects of age and rapid high-pressure fixation on the morphology of Schlemm's canal. Invest Ophthalmol Vis Sci 1990;31:745-750.
50. Grierson I, Howes RC, Wang Q. Age-related changes in the canal of Schlemm. Exp Eye Res 1984;39:505-512.
51. Overby DR, Zhou EH, Vargas-Pinto R, et al. Altered mechanobiology of Schlemm's canal endothelial cells in glaucoma. Proc Natl Acad Sci U S A 2014;111:13876-13881.
52. Stamer WD, Braakman ST, Zhou EH, et al. Biomechanics of Schlemm's canal endothelium and intraocular pressure reduction. Prog Retin Eye Res 2015;44:86-98.
53. Zhou EH, Krishnan R, Stamer WD, et al. Mechanical responsiveness of the endothelial cell of Schlemm's canal: scope, variability and its potential role in controlling aqueous humour outflow. J R Soc Interface 2012;9:1144-1155.
54. Gong H, Tripathi RC, Tripathi BJ. Morphology of the aqueous outflow pathway. Microsc Res Tech 1996;33:336-367.
55. Nesterov AP, Hasanova NH, Batmanov YE. Schlemm's canal and scleral spur in normal and glaucomatous eyes. Acta Ophthalmol (Copenh) 1974;52:634-646.
56. Rohen JW, Lütjen E, Bárány E. The relation between the ciliary muscle and the trabecular meshwork and its importance for the effect of miotics on aqueous outflow resistance. A study in two contrasting monkey species, Macaca irus and Cercopithecus aethiops. Albrecht Von Graefes Arch Klin Exp Ophthalmol 1967;172:23-47.
57. Nishida S, Mizutani S. Topography of the human ciliary muscle. Nihon Ganka Gakkai Zasshi 1991;95:1044-1056.
58. Moses RA, Arnzen RJ. The trabecular mesh: a mathematical analysis. Invest Ophthalmol Vis Sci 1980;19:1490-1497.
59. Kaufman PL, Bárány EH. Loss of acute pilocarpine effect on outflow facility following surgical disinsertion and retrodisplacement of the ciliary muscle from the scleral spur in the cynomolgus monkey. Invest Ophthalmol 1976;15:793-807.
60. Tamm ER, Koch TA, Mayer B, Stefani FH, Lütjen-Drecoll E. Innervation of myofibroblast-like scleral spur cells in human monkey eyes. Invest Ophthalmol Vis Sci 1995;36:1633-1644.
61. Tamm E, Flügel C, Stefani FH, Rohen JW. Contractile cells in the human scleral spur. Exp Eye Res 1992;54:531-543.
62. Johnson M, Erickson K. Mechanisms and routes of aqueous humor drainage. In: Albert D, Jokbiec F (eds), Principles and practice of ophthalmology. Philadelphia: WB Saunders Co; 2000:2577-2595.
63. Li G, Farsiu S, Chiu SJ, et al. Pilocarpine-induced dilation of Schlemm's canal and prevention of lumen collapse at elevated intraocular pressures in living mice visualized by OCT. Invest Ophthalmol Vis Sci 2014;55:3737-3746.
64. Swain DL, Ho J, Lai J, Gong H. Shorter scleral spur in eyes with primary open-angle glaucoma. Invest Ophthalmol Vis Sci 2015;56:1638-1648.
65. Moses RA, Grodzki WJ. The scleral spur and scleral roll. Invest Ophthalmol Vis Sci 1977;16:925-931.
66. Grierson I, Lee WR, Abraham S. Effects of pilocarpine on the morphology of the human outflow apparatus. Br J Ophthalmol 1978;62:302-313.
67. Liu S, Li H, Dorairaj S, et al. Assessment of scleral spur visibility with anterior segment optical coherence tomography. J Glaucoma 2010;19:132-135.
68. Cumba RJ, Radhakrishnan S, Bell NP, et al. Reproducibility of scleral spur identification and angle measurements using fourier domain anterior segment optical coherence tomography. J Ophthalmol 2012;2012:487309.
69. McKee H, Ye C, Yu M, Liu S, Lam DS, Leung CK. Anterior chamber angle imaging with swept-source optical coherence tomography: detecting the scleral spur, Schwalbe's Line, and Schlemm's Canal. J Glaucoma 2013;22:468-472.
70. Seager FE, Wang J, Arora KS, Quigley HA. The effect of scleral spur identification methods on structural measurements by anterior segment optical coherence tomography. J Glaucoma 2014;23:e29-38.
71. Johnstone MA, Grant WM. Microsurgery of Schlemm's canal and the human aqueous outflow system. Am J Ophthalmol 1973;76:906-917.
72. Battista SA, Lu Z, Hofmann S, Freddo T, Overby DR, Gong H. Reduction of the available area for aqueous humor outflow and increase in meshwork herniations into collector channels following acute IOP elevation in bovine eyes. Invest Ophthalmol Vis Sci 2008;49:5346-5352.
73. Moses RA, Grodzki WJ, Etheridge EL, Wilson CD. Schlemm's canal: the effect of intraocular pressure. Invest Ophthalmol Vis Sci 1981;20:61-68.
74. Van Buskirk EM. Anatomic correlates of changing aqueous outflow facility in excised human eyes. Invest Ophthalmol Vis Sci 1982;22:625-632.
75. Moses RA. Circumferential flow in Schlemm's canal. Am J Ophthalmol 1979;88:585-591.
76. Zhu JY, Ye W, Wang T, Gong HY. Reversible changes in aqueous outflow facility, hydrodynamics, and morphology following acute intraocular pressure variation in bovine eyes. Chin Med J (Engl) 2013;126:1451-1457.
77. Gong H, Francis A. Schlemm's canal and collector channels as therapeutic targets. In: Samples J, Ahmed I (eds), Innovations in Glaucoma Surgery. pp. 3-25. New York: Springer; 2014.
78. Allingham RR, de Kater AW, Ethier CR. Schlemm's canal and primary open-angle glaucoma: correlation between Schlemm's canal dimensions and outflow facility. Exp Eye Res 1996;62:101-109.
79. Hann CR, Vercnocke AJ, Bentley MD, Jorgensen SM, Fautsch MP. Anatomic changes in Schlemm's canal and collector channels in normal and primary open-angle glaucoma eyes using low and high perfusion pressures. Invest Ophthalmol Vis Sci 2014;55:5834-5841.
80. Hong J, Xu J, Wei A, et al. Spectral-domain optical coherence tomographic assessment of Schlemm's canal in Chinese subjects with primary open-angle glaucoma. Ophthalmology 2013;120:709-715.
81. Johnson DH, Matsumoto Y. Schlemm's canal becomes smaller after successful filtration surgery. Arch Ophthalmol 2000;118:1251-1256.

82. Johnstone MA, Grant WG. Pressure-dependent changes in structures of the aqueous outflow system of human and monkey eyes. Am J Ophthalmol 1973;75:365-383.
83. Brubaker RF. The effect of intraocular pressure on conventional outflow resistance in the enucleated human eye. Invest Ophthalmol 1975;14:286-292.
84. Gong H, Gorantla V, Zhang Y, Freddo T, Swain D. Morphological changes in the distal outflow pathway of primary open-angle glaucoma. Invest Ophthalmol Vis Sci 2015;56:3300.
85. Hann CR, Fautsch MP. Preferential fluid flow in the human trabecular meshwork near collector channels. Invest Ophthalmol Vis Sci 2009;50:1692-1697.
86. Grieshaber MC, Pienaar A, Olivier J, Stegmann R. Clinical evaluation of the aqueous outflow system in primary open-angle glaucoma for canaloplasty. Invest Ophthalmol Vis Sci 2010;51:1498-1504.
87. Lu Z, Overby DR, Scott PA, Freddo TF, Gong H. The mechanism of increasing outflow facility by rho-kinase inhibition with Y-27632 in bovine eyes. Exp Eye Res 2008;86:271-281.
88. Lu Z, Zhang Y, Freddo TF, Gong H. Similar hydrodynamic and morphological changes in the aqueous humor outflow pathway after washout and Y27632 treatment in monkey eyes. Exp Eye Res 2011;93:397-404.
89. Hann CR, Bahler CK, Johnson DH. Cationic ferritin and segmental flow through the trabecular meshwork. Invest Ophthalmol Vis Sci 2005;46:1-7.
90. Chang JY, Folz SJ, Laryea SN, Overby DR. Multi-scale analysis of segmental outflow patterns in human trabecular meshwork with changing intraocular pressure. J Ocul Pharmacol Ther 2014;30:213-223.
91. Keller KE, Bradley JM, Vranka JA, Acott TS. Segmental versican expression in the trabecular meshwork and involvement in outflow facility. Invest Ophthalmol Vis Sci 2011;52:5049-5057.
92. Vranka JA, Bradley JM, Yang YF, Keller KE, Acott TS. Mapping molecular differences and extracellular matrix gene expression in segmental outflow pathways of the human ocular trabecular meshwork. PLoS One 2015;10:e0122483.
93. Yang CY, Liu Y, Lu Z, Ren R, Gong H. Effects of Y27632 on aqueous humor outflow facility with changes in hydrodynamic pattern and morphology in human eyes. Invest Ophthalmol Vis Sci 2013;54:5859-5870.
94. Melamed S, Epstein DL. Alterations of aqueous humour outflow following argon laser trabeculoplasty in monkeys. Br J Ophthalmol 1987;71:776-781.
95. Epstein DL, Rohen JW. Morphology of the trabecular meshwork and inner-wall endothelium after cationized ferritin perfusion in the monkey eye. Invest Ophthalmol Vis Sci 1991;32:160-171.
96. Cha EDK, Xu J, Gong H. Variations in active areas of aqueous humor outflow through the trabecular outflow pathway. Invest Ophthalmol Vis Sci 2015;56:4850.
97. Swaminathan SS, Oh DJ, Kang MH, et al. Secreted protein acidic and rich in cysteine (SPARC)-null mice exhibit more uniform outflow. Invest Ophthalmol Vis Sci 2013;54:2035-2047.
98. Gong H, Yang CY. Morphological and hydrodynamic correlations with increasing outflow facility by rho-kinase inhibitor Y-27632. J Ocul Pharmacol Ther 2014;30:143-153.
99. Zhang Y, Toris CB, Liu Y, Ye W, Gong H. Morphological and hydrodynamic correlates in monkey eyes with laser induced glaucoma. Exp Eye Res 2009;89:748-756.
100. Cha E, Jin R, Gong H. The relationship between morphological changes and reduction of active areas of aqueous outflow in eyes with primary open-angle glaucoma. Invest Ophthalmol Vis Sci 2013;54:2291.
101. Gong H, Cha EDK, Gorantla V, et al. Characterization of aqueous humor outflow through novel glaucoma devices – a tracer study. Invest Ophthalmol Vis Sci 2012;53:3743.